

Review

# Supported Palladium Nanocatalysts: Recent Findings in Hydrogenation Reactions

Marta A. Andrade  and Luísa M. D. R. S. Martins \* 

Centro de Química Estrutural, Instituto Superior Técnico, Universidade de Lisboa, 1049-001 Lisboa, Portugal; marta.andrade@tecnico.ulisboa.pt

\* Correspondence: luisammartins@tecnico.ulisboa.pt; Tel.: +351-218419389

Received: 7 August 2020; Accepted: 12 September 2020; Published: 17 September 2020



**Abstract:** Catalysis has witnessed a dramatic increase on the use of metallic nanoparticles in the last decade, opening endless opportunities in a wide range of research areas. As one of the most investigated catalysts in organic synthesis, palladium finds numerous applications being of significant relevance in industrial hydrogenation reactions. The immobilization of Pd nanoparticles in porous solid supports offers great advantages in heterogeneous catalysis, allowing control of the major factors that influence activity and selectivity. The present review deals with recent developments in the preparation and applications of immobilized Pd nanoparticles on solid supports as catalysts for hydrogenation reactions, aiming to give an insight on the key factors that contribute to enhanced activity and selectivity. The application of mesoporous silicas, carbonaceous materials, zeolites, and metal organic frameworks (MOFs) as supports for palladium nanoparticles is addressed.

**Keywords:** nanoparticles; palladium; hydrogenation; catalyst; supported; mesoporous silica; carbon material; zeolite; MOF

## 1. Introduction

Throughout the last two decades, nanoparticles (NPs) emerged as a new type of important functional material, playing a major role in several areas, from electronics to the development of composite materials [1,2]. NPs, or ultrafine particles, are usually defined as particles of matter with one or more dimensions (length, width, or thickness) that fall within the nanometer size range, that is, between 1 and 100 nanometers (nm). Among these, metallic NPs (MNPs) have attracted the attention of the scientific community owing to their high surface-to-volume area, selectivity, easy to tune morphologies, and significant catalytic activity [3–6].

The last decade has seen a significant boost on the application of MNPs in several fields, with a significantly high number of contributions (*ca.* 17,700 contributions in the period 2010–July 2020). One of the main reasons for the rapidly expanding area of MNPs synthesis is the encouraging results obtained in catalysis [6,7]. From this universe, 37% of the reported studies correspond to applications with palladium NPs (Figure 1). Pd exhibits a highly versatile reactivity, finding numerous industrial applications on fine chemicals production [5]. Palladium nanoparticles (PdNPs) are one of the most important and fascinating nanomaterials, inducing different types of activation, but playing a key role in hydrogenation processes.

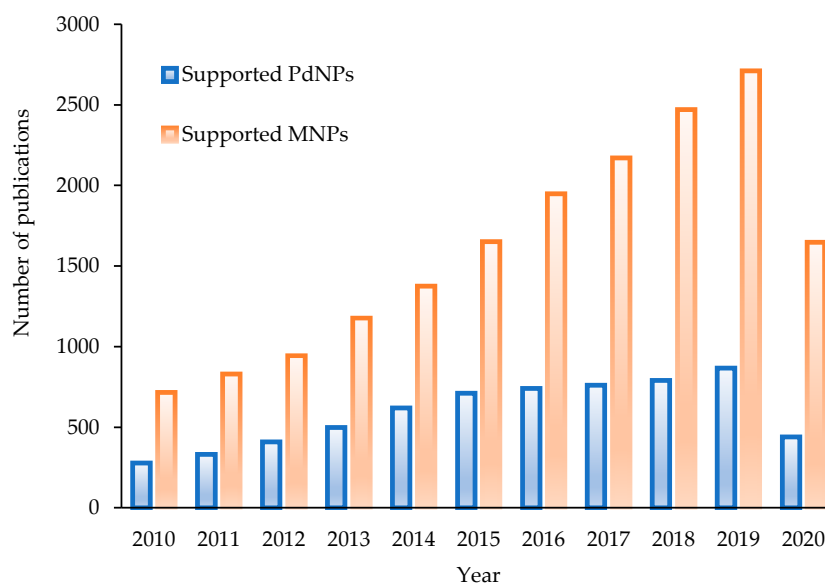


**Figure 1.** Rising interest on the development of supported palladium nanoparticles (PdNPs) and metallic NPs (MNPs). Topics: (metal nanoparticles and supported and catalysis. Analysis: publication years: (2010 to 2020) and research areas: (chemistry, materials science, science technology other topics, engineering, physics, energy fuels, electrochemistry, environmental sciences, ecology, polymer science). Source: ISI Web of Knowledge, accessed on 25, July 2020.

The synthesis of PdNPs has been the subject of intensive investigation over the two past decades, with emphasis on the key parameters that directly impact its catalytic activity as size and morphology control of the as-prepared particles. The multipurpose reactivity of PdNPs finds its origin in its ability for stabilizing different species exhibiting different oxidation states in the reaction medium, and also to the distinctive reactivity of the extended metal surface. Due to their high surface energy, PdNPs tend to become thermodynamically unstable and susceptible to aggregation during catalysis, leading to an activity loss. The synthesis of heterogenized catalysts calls for robust immobilization strategies that can effectively control the size, shape, and dispersion of PdNPs; thus, achieving high and stable activity.

This short review covers some of the latest developments for supported PdNPs, highlighting some new easy approaches for their preparation, as well as green synthesis approaches. The catalytic performance of the supported PdNPs towards hydrogenation reactions is addressed, exploring the key factors for catalytic activity and selectivity enhancement.

## 2. Hydrogenation and Hydrogen Transfer Processes

Hydrogenation reactions stand as fundamental transformations for the industrial production of fine and bulk hydrogenated compounds [8,9]. Hydrogenation reactions catalyzed by metal species have drawn attention of the scientific community for most of the 20th century, given their significance in the industrial production of chemicals [10]. Reduction reactions of various functionalities are of considerable relevance for the industrial synthesis of intermediates or the transformation of fine chemicals. For instance, alcohols are formed upon ketones, aldehydes, and esters hydrogenation, and the reduction of alkenes and alkynes, resulting in aliphatic compounds or alkanes. Likewise, nitro compounds, as well as nitriles, can be converted into amines.

Hydrogenation reactions can follow two strategies, either direct hydrogenation with  $H_2$  gas or transfer hydrogenation, involving the presence of a non- $H_2$  hydrogen species [11,12]. Transfer hydrogenation is a suitable and effective method to obtain hydrogenated compounds, and an appealing substitute to direct hydrogenation processes, being recently the focus of research in this field. Even though various immobilized metals catalyze the several hydrogenation reactions, they are not very selective in the presence of more than one reducible group.

Well-defined PdNPs have proved their selectivity and efficiency towards the hydrogenation of olefins, even for reactions such as the hydrogenation of arenes, weakly catalyzed by metallic species [13,14]. Pd-based nanocatalysts are therefore effective for several hydrogenation reactions due to its ability to combine with a wide array of ligands, showing high selectivity. Investigation on this topic is more directed towards immobilized PdNPs due to faster reaction rates and excellent efficiencies.

### 3. PdNPs@supports

The reuse of costly metal particles is of foremost interest from both economic and environmental perspectives. The need for more eco-friendly and cost-effective technology has combined efforts to the development of more efficient, selective and recyclable catalytic systems.

An enhancement of the catalytic efficiency requires improvement in the activity and selectivity. Immobilized catalysts benefit from an increase of the surface and porous volume of the composite that effectively can enhance both activity and selectivity in heterogeneous systems [15–17]. The selection of a suitable stable solid support is the most important step for MNPs immobilization (Figure 2). Distinct approaches for the preparation of effective and recyclable PdNPs catalysts have been reported in the literature, involving a large variety of solid supports, as carbon-based materials [7,18,19], silicas [20–22], metal organic frameworks (MOFs) [23–25], zeolites [26–28], and also metal oxides, polymers, or magnetic composites [1,29], among the most used.

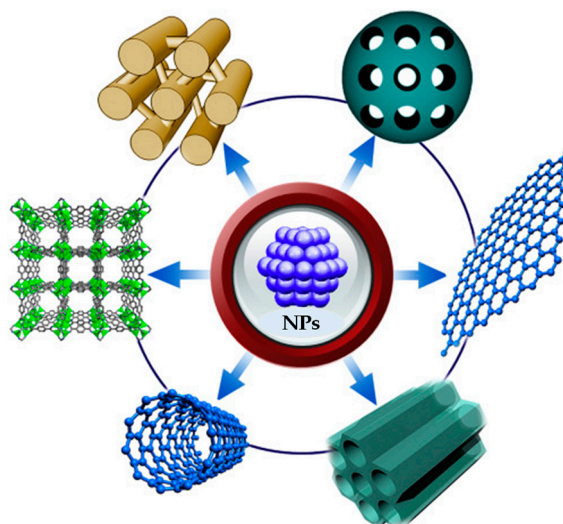


**Figure 2.** Immobilization of MNPs to various high surface area materials. Adapted with permission from Zhu et al. [30], *Chem*; published by Elsevier Inc., 2016.

These above-mentioned materials usually display high surface areas, which combined with their distinctive surface chemistry, can deliver exceptional selectivity, through the customized design of the catalysts. In addition, aggregation or precipitation phenomena that can lead to a loss of catalytic activity of the PdNPs can be reduced and controlled using stabilizers as ligands, surfactants, or polymers. Typical procedures for the preparation of PdNPs immobilized in high porous materials include more conventional methods that generally include precipitation and infiltration approaches, and subsequent reduction of the Pd precursor [7]. Recent advances are mainly based on the use of superior techniques for the incorporation of Pd precursors into the porosity of the supports and on modification of the surface of support material for enhanced support-metal interactions. These strategies include incipient wetness impregnation, double-solvent use, chemical vapor deposition, solvent-free solid grinding, among others.

Biomass-derived supported PdNPs have captured the interest of researchers given their eco-friendly, sustainable, and economical nature. These biomass-derived supports are acknowledged

as valuable nanocatalysts in several catalytic reactions because of the high activity and selectivity displayed, minimizing toxic substances [31,32].

Supported PdNPs are one of the most used and efficient catalysts in hydrogenation reactions [33]. Nanoparticles are bound either mechanically or chemically to the support surface, while catalysis is carried out in a heterogeneous system. The advantages of both heterogeneous and homogeneous catalysis [22,34], allow a facile separation of the catalyst, an ease of the recyclability in the system, and a protection from catalyst deactivation and degradation [7]. However, activity and selectivity can be affected negatively due to the principles of diffusion and the engagement of two different phases in the reaction [35].

From the above-mentioned materials, the use of zeolites, carbon materials, MOFs and mesoporous silicas for PdNPs immobilization, will be discussed in more detail in the next sections covering some recent examples in the literature.

#### 4. PdNPs@silicas

Owing to its excellent thermal stability, silica NPs are promising supports for MNPs immobilization. The use of these materials as catalyst supports, presents major advantages given its features as high surface areas and widely accessible porous network [20,36,37]. Their well-ordered channel structures presenting tunable porosity over a wide range and the abundance of surface silanol groups facilitates its covalently mediated functionalization, thus, stabilizing the resulting MNPs. The potentialities of mesoporous silicas (MS) as supports in numerous reactions, as hydrogenation, alkylation, and oxidation of several substrates have been widely acknowledged [7,30,38]. Common approaches for the immobilization of MNPs into MS include methods as solution infiltration and incipient wetness impregnation lack, however, control growth of MNPs. The incorporation of PdNPs within MS supports by a post-synthetic deposition method makes the control of the particle size and dispersion of PdNPs more difficult. Conversely, the use of a direct synthesis method, through the in-situ incorporation of the metal precursors can yield uniformly distributed confined PdNPs, the reason for the more recent research. Other topics of research are focused on mesopore size enlargement, and on the role of the silica structure as support, as pore size and morphology that can optimize the catalytic performance. Importantly, the introduction of stabilizing and structure-directing agents in the direct synthesis approach has also been investigated. The following examples are recent contributions on this field, covering some of the above-mentioned topics.

The influence of a structure-directing agent, 1,3,5-trimethylbenzene (TMB) on the in-situ incorporation of PdNPs within MS was explored by Yu and colleagues [38]. Pd-MS catalysts were synthesized, with and without the addition of TMB, by the direct synthesis method with Pd incorporated in MS, under basic conditions (Figure 3). The average sizes for PdNPs obtained by the direct synthesis method were much smaller (2.4–4.3 nm) than those synthesized by a post-synthetic deposition method (17.7 nm for Pd/(MS-50)), as confirmed by Transmission Electron Microscopy (TEM).

An increase in the Pd loading of the catalysts was observed for increasing pH, being attributed to the charge density increase of silicates, which results in a higher  $\text{Pd}^{2+}$  ions adsorption and uniform dispersion within the silica species. All the Pd-MS-x-TMB catalysts (x: amount of added  $\text{NH}_3$ ), exhibited disorderly worm-like porous structures, unlike Pd-MS-50 that displayed ordered linear channels. The  $\text{N}_2$  adsorption data confirmed the existence of mesoporous structure. The influence of TMB as an expanding agent, and also as a structure-directing agent, resulted in the formation of MS with larger pore diameter and pore volume, as well in a worm-like morphology. Pd introduction into a pre-synthesized MS resulted in a somewhat larger pore size. X-ray Photoelectron Spectroscopy (XPS) studies confirmed the presence of metallic Pd in Pd/(MS-50).



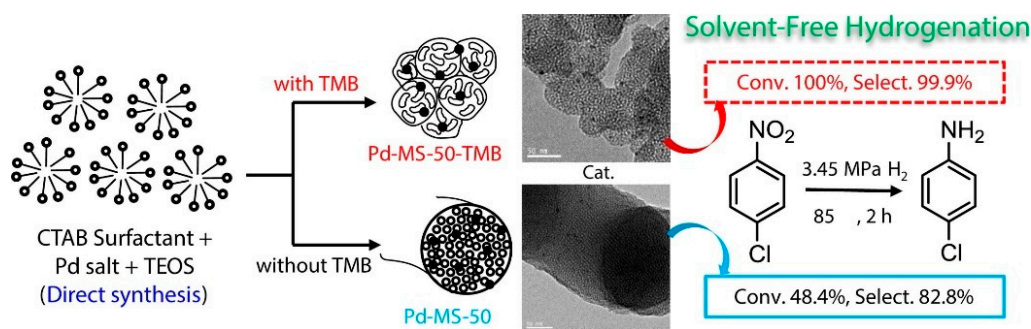


**Figure 3.** Preparation of Pd-mesoporous silicas (MS) catalysts and major catalytic outcomes for the solvent-free application to hydrogenation of *p*-chloronitrobenzene. Reproduced with permission from Yu et al., *Chemical Engineering Journal*; published by Elsevier B.V., 2017.

The hydrogenation of *p*-chloronitrobenzene (CNB) over Pd-MS catalysts was studied (Table 1), in terms of *p*-CNB conversion, and selectivity to *p*-chloroaniline (*p*-CAN), and aniline (AN). The conversion obtained for Pd-MS-50-TMB was much higher than that observed for Pd/(MS-50) due to a higher dispersion of PdNPs. Furthermore, catalyst Pd-MS-50-TMB showed a better catalytic performance than Pd-MS-50, most likely related to the particle size, larger porosity and also to the worm-like morphology of MS, which allows an easier accessibility of reactants to the active incorporated Pd in the catalytic sites, enhancing mass transfer process [39]. The catalytic activity for Pd-MS-xx-TMB catalysts for *p*-CNB hydrogenation highlighted the importance of increasing pH.

**Table 1.** Textural properties of the Pd-MS catalysts and catalytic data for the solvent-free hydrogenation of *p*-chloronitrobenzene (*p*-CNB) [38].

Catalyst	$A_{\text{BET}}$ ( $\text{m}^2\text{g}^{-1}$ )	$V_{\text{p}}$ ( $\text{cm}^3\text{g}^{-1}$ )	$D_{\text{p}}$ (nm)	Pd Loading (%)	<i>p</i> -CNB Conversion (%)	Selectivity (%)	
						<i>p</i> -CAN	AN
Pd-MS-05-TMB	873	1.29	3.7	0.16	28.2	71.6	28.4
Pd-MS-10-TMB	912	1.33	3.5	0.45	41.9	94.1	5.9
Pd-MS-30-TMB	980	1.43	3.3	0.54	59.7	95.3	4.7
Pd-MS-50-TMB	854	1.06	3.8	0.67	100	99.9	0.1
Pd-MS-50	919	0.07	2.6	0.73	48.4	82.8	17.2
Pd/(MS-50)	687	0.43	2.5	0.68	29.5	97.6	2.4

The conversion of *p*-CNB using the Pd/SiO<sub>2</sub> catalyst was much lower (6.1%) than that obtained for Pd/(MS-50) catalyst, also indicating that a larger porosity and pore volume was more beneficial for the reaction. Complete conversion of *p*-CNB with selectivity over 99.5% was accomplished in the first three cycles in recycling studies for Pd-MS-50-TMB. In the fifth cycle, a conversion and selectivity to *p*-CAN drop was observed due to coke deposition. The Pd-MS-50-TMB catalyst was regenerated [40], leading to its complete restoration.

In 2017, Sun and colleagues reported the preparation of MS-based nanotubes supported PdNPs [41], using different framework structures, as organic groups and carbon/silica hybrids. The synthesis of silica nanotubes (SNT) containing ethylene or phenylene groups, E-SNT and B-SNT, respectively, was performed in accordance with a previously method reported by the authors with minor modifications (Figure 4, top) [42]. The authors used a much lower surfactant concentration than that used for the synthesis of SBA-15, which was advantageous to obtain a rod-like micelle formation. The carbon-doped silica nanotubes E-CS-NT and B-CS-NT were carbonized at 800 °C in N<sub>2</sub> atmosphere for 2 h (CS: carbon/silica hybrid). In addition, the pristine (SNT) and SBA-15 were also synthesized. The nanotube morphology of E-SNT and B-SNT, was maintained after calcination although narrower

diameters were observed. PdNPs were uniformly dispersed in the distinct nanotubes by means of an impregnation-reduction process.

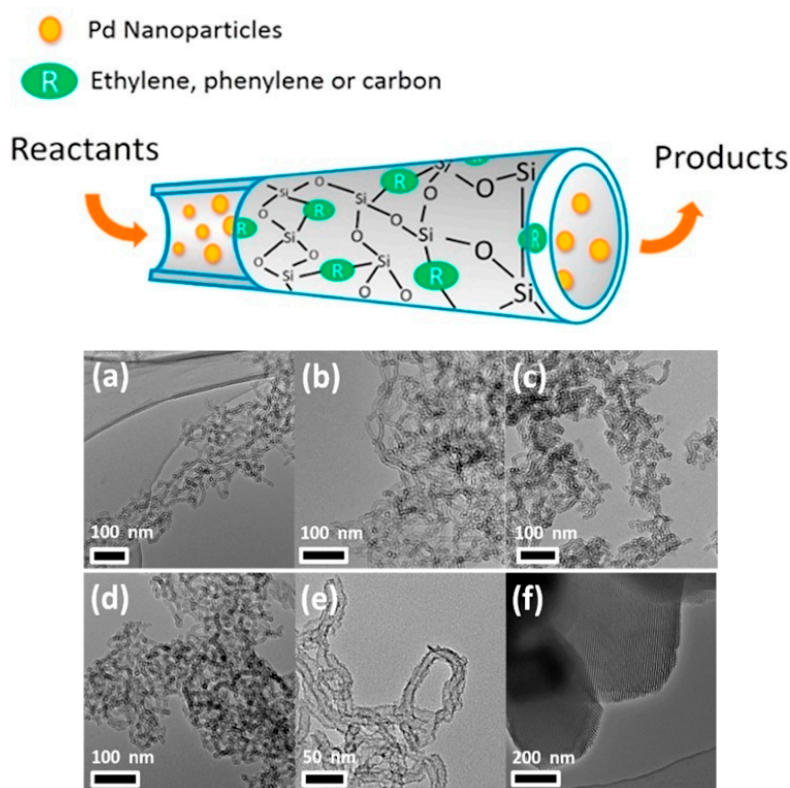


**Figure 4.** Top: Illustrated scheme of Pd supported ethylene, phenylene bridged or carbon doped organosilica nanotubes and reaction process. Bottom: TEM images of (a) E-silica nanotubes (SNT), (b) B-SNT, (c) E-CS-NT, (d) B-CS-NT, (e) SNT, and (f) SBA-15. Reproduced with permission from Sun et al., *Microporous and Mesoporous Materials*; published by Elsevier B.V., 2017.

The nanotube structure is clearly observed in the TEM images (Figure 4, bottom), displaying internal diameters with less than 10 nm for E-SNT and B-SNT. The textural analysis indicates the formation of a mesoporous structure and assembling pores by nanotubes. Apparent surface areas were lower upon calcination, with a noteworthy pore size decrease from E-SNT and B-SNT to the corresponding E-CS-NT and B-CSNT (from 7.3 and 6.0 nm to 4.5 and 4.0 nm), ascribed to nanotubes shrinkage. The carbon content in E-CS-NT and B-CS-NT was of 10% and 20%, respectively. The silica-based materials loaded PdNPs also showed a spherical morphology with 2–4 nm particles, dispersed uniformly in the inner porosity of the catalysts. Relatively larger PdNPs (5 nm) were observed for SNT and SBA-15. Additionally, deposition of PdNPs on amorphous silica resulted in 10 nm mean size NPs, demonstrating the confinement effect of the nanotube structure on the Pd agglomeration. Similar type IV isotherms were obtained after the nanotube encapsulation of PdNPs, pointing out the integrity of the nanotube structure. The presence of both metallic and oxidized states of Pd, with Pd(0) contents of 50–62% was confirmed by XPS.

The catalytic performance of the silica-based nanotubes loaded PdNPs towards the hydrogenation of  $\alpha,\beta$ -unsaturated carboxylic acids was investigated in the presence of the chiral modifier cinchonidine (Figure 5), achieving a conversion of 99% of  $\alpha$ -phenyl cinnamic acid within 10 h at room temperature, and  $H_2$  pressure of 0.1 MPa for encapsulated PdNPs in the B-SNT, E-SNT, and E-CS-NT, respectively (Table 2).

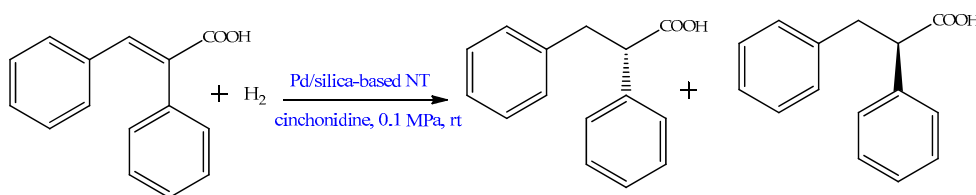


**Figure 5.** Scheme for the enantioselective hydrogenation reaction of  $\alpha,\beta$ -unsaturated carboxylic acids.

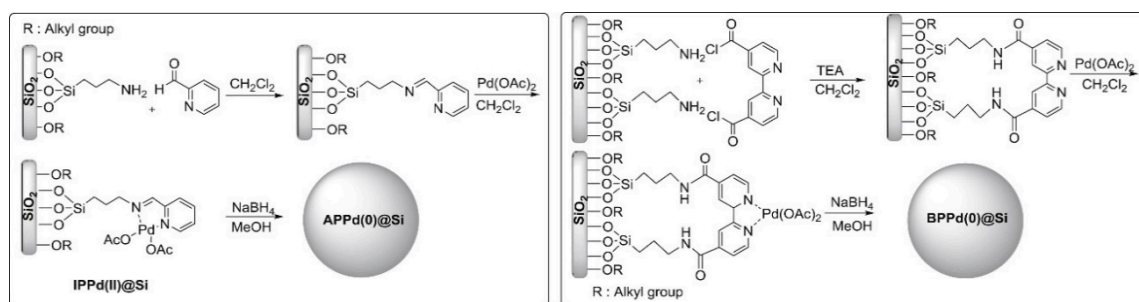
**Table 2.** Catalytic performance of the Pd supported catalysts for the enantioselective hydrogenation of  $\alpha,\beta$ -unsaturated carboxylic acid [41].

Catalyst	Conversion (%)	ee * (%)
Pd/E-SNT	>99	40
Pd/B-SNT	>99	48
Pd/E-CS-NT	>99	30
Pd/SNT	46	33
Pd/CNT	-	51

\*- enantiomeric excess.

The hydrophobicity of SNT with organic groups may enhance the preferential adsorption of  $\alpha$ -phenyl cinnamic acid and cinchonidine, to the Pd active center, increasing the activity. In fact, the high activity and enantioselectivity can be explained by the fast adsorption of chiral modifiers and reactants [43]. Conversely, the hydrophilic properties of SNT resulted in the lowest activity. The excellent catalytic activity towards the enantioselective hydrogenation of  $\alpha,\beta$ -unsaturated carboxylic acids clearly benefits from the particular morphology of the catalysts and also from the hydrophobic/hydrophilic properties of the surface.

Shabbir and Lee applied two catalytic systems of reverse phase amino functionalized silica supported PdNPs to the hydrogenation reaction of *trans*-cinnamic acid and similar compounds in water [44]. Two types of silica-supported Pd(0) catalysts were synthesized by the modification of the commercial 3-aminopropyl-functionalized silica gel using 2-pyridinecarboxaldehyde ligand and bipyridyl ligand (Figure 6). The amino-functionalized reverse phase silica induced hydrophobicity in the polar silica support. After silica modification, coordination of Pd(II) was performed, with reduction to PdNPs, yielding APPd(0)@Si and BPPd(0)@Si catalysts (Figure 6), with average PdNPs size of around 3 and 4 nm and Pd(0) loadings of  $0.540 \text{ mmol g}^{-1}$  and  $0.598 \text{ mmol g}^{-1}$  for APPd(0)@Si and BPPd(0)@Si, respectively. The pore size of 6–8 nm of the catalysts is quite similar to that of the commercial silica gel.

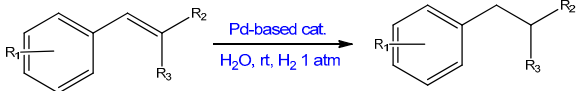


**Figure 6.** Synthetic procedure of APPd(0)@Si and BPPd(0)@Si. Reproduced with permission from Shabbir et al., *Journal of Organometallic Chemistry*; published by Elsevier B.V., 2017.

The synthesized catalysts were tested in the hydrogenation reaction of *trans*-cinnamic acid and related compounds. A selection of available bases at different temperatures was tested to optimize the reaction conditions (Table 3). KOH proved to be a good choice as opposed to potassium carbonate. The newly synthesized catalysts outperformed the commercial catalyst Pd/C at a 5.0% molar ratio,

45% of product yields. The hydrogenation of several  $\alpha,\beta$ -unsaturated carbonyl compounds was also investigated for by BPPd(0)@Si and APPd(0)@Si, achieving efficient completion. Yields >95% were observed for the hydrogenation of all the unsaturated esters, ketones and alcohols. After the reaction, both APPd(0)@Si and BPPd(0)@Si were also recycled, showing good stability with negligible leaching of PdNPs.

**Table 3.** Hydrogenation catalyzed by APPd(0)@Si and BPPd(0)@Si catalysts [44].

				
R <sub>1</sub> , R <sub>2</sub> , R <sub>3</sub>	Catalyst (mol %)	Base	Time (h)	TOF * (h <sup>-1</sup> )
a (-H, -COOH, -H)	BPPd(0)@Si (1)	KOH	0.5	126
a	BPPd(0)@Si (3)	KOH	0.5	58
a	APPd(0)@Si (5)	KOH	0.5	40
a	BPPd(0)@Si (1)	KOH	0.5	40
a	BPPd(0)@Si (5)	K <sub>2</sub> CO <sub>3</sub>	0.5	32.4
b (-H, -COCH <sub>3</sub> , -H)	BPPd(0)@Si (5)	-	1	20
b	Pd/C (5)	-	1	9
c (-H, -CH <sub>2</sub> OH, -H)	BPPd(0)@Si (5)	-	0.5	23.2
c	APPd(0)@Si (5)	-	0.5	18.8
c	BPPd(0)@Si (5)	-	2	10
c	APPd(0)@Si (5)	-	2	10

\* Turnover Frequency.

Rungsi and colleagues explored the influence of the silica source used on the hydrothermal preparation of MCM-41, followed by PdNPs impregnation on the mesoporous MCM-41 supports [45] and application in the catalytic partial hydrogenation of soybean-derived polyunsaturated fatty acid methyl esters (FAMES), as displayed in Figure 7. The microwave-assisted synthesis of mesoporous MCM-41 silica, using fumed silica (SiO<sub>2</sub>) and silatrane (Si(TEA)<sub>2</sub>) as silica sources, significantly shortened the hydrotreatment time. MCM-41 product has shown much higher values regarding its textural parameters, as MCM-41-SiO<sub>2</sub> support and MCM-41-silatrane, than reported elsewhere [46].

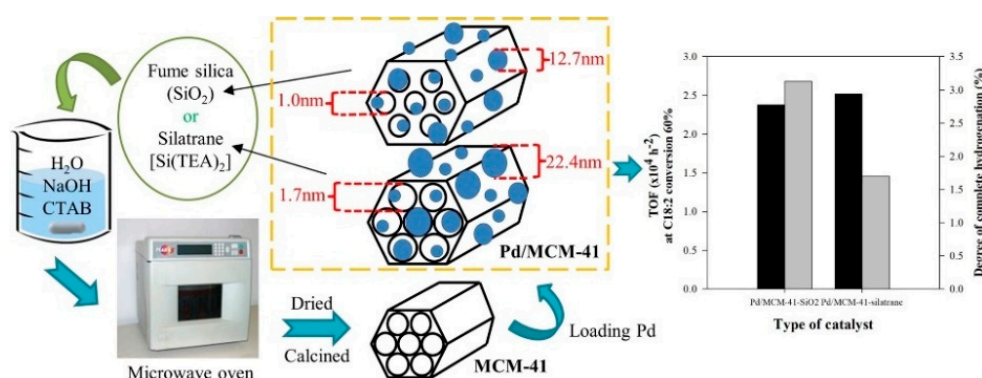


**Figure 7.** Schematic procedure of the preparation of Pd/MCM-41 catalysts and hydrogenation results. Reproduced with permission from Rungsi et al., Applied Catalysis A: General; published by Elsevier B.V., 2018.

The small-angle X-ray diffraction (XRD) patterns disclosed well-ordered mesostructures for MCM-41-SiO<sub>2</sub>, unlike MCM-41-silatrane. After Pd impregnation, a less ordered structure was observed. For the same weight content, a good Pd dispersion was obtained for the MCM-41-SiO<sub>2</sub> support. The values obtained for the textural parameters have shown a slight decrease, suggesting the

location of PdNPs on the external surface and in some pores due to the migration of some species in the framework. MCM-41-silatrane presented a narrower pore size distribution compared to MCM-41-SiO<sub>2</sub>. Supported palladium was Pd(0), as revealed by X-ray Photoelectron Spectroscopy (XPS).

The catalytic properties of PdNPs supported on MCM-41 for the partial hydrogenation of soybean oil-based FAMES were investigated. Both catalysts presented fast and selective conversions to monounsaturated fatty acid methyl esters, although Pd/MCM-41-silatrane has shown a higher catalytic performance due to its greater stability and higher surface of Pd active sites. Overall, the catalytic activity of Pd/MCM-41 is attributed to its suitable size and density of metallic active sites, which subsequently determine the catalytic reactivity and selectivity.

Ganji and colleagues investigated for the first time a carboxylic acid functionalized SBA-15 derived Pd nanocatalyst towards the selective catalytic hydrogenation of nitrobenzene in water medium [47]. The synthesis of SBA-15 and SBA-COOH followed reported procedures [48,49] and the preparation of Pd/SBA-COOH catalyst was achieved through dispersion of SBA-COOH in a palladium acetate solution followed by reduction with NaBH<sub>4</sub>. XRD of Pd/SBA-COOH catalyst revealed characteristic peaks of very small Pd particles. All the Pd species present in the Pd/SBA-COOH catalyst were Pd(0), as confirmed by XPS. SBA-15, SBA-COOH, and Pd/SBA-COOH exhibited type IV N<sub>2</sub> adsorption isotherms with an H1 hysteresis loop [50]. After modification with the -COOH group and PdNPs, a decrease of textural parameters was observed when compared to pristine SBA-15. The TEM images of the Pd/SBA-COOH nanocomposites revealed the well-ordered mesoporous channel structure of the SBA-15 silica materials, as well as the spherical morphology of the 3.5 nm-sized and highly dispersed (32%) PdNPs in the SBA-15 channels. The catalytic activity of Pd/SBA-COOH was studied towards nitrobenzene hydrogenation using hydrazine hydrate, N<sub>2</sub>H<sub>4</sub> (Table 4).

**Table 4.** Hydrogenation of nitrobenzene with the different catalysts [47].

Catalyst	N <sub>2</sub> H <sub>4</sub> ·H <sub>2</sub> O (equiv.)	Conversion (%)	Selectivity (%)
SBA-15	2	-	-
SBA-COOH	2	-	-
Pd/SBA-15	2	68	100
Pd/SBA-COOH	0.5	5	100
Pd/SBA-COOH	1	44	100
Pd/SBA-COOH	1.5	76	100
Pd/SBA-COOH	2	100	100

The enhanced catalytic activity observed for Pd/SBA-COOH is most likely due to the highly dispersed smaller-sized PdNPs. A synergistic effect is observed between the SBA-COOH support and its textural parameters, as previously reported in the literature [51]. The hydrogenation reaction of nitrobenzene showed much lower efficiencies in various organic solvents than that obtained under solvent-free conditions (Figure 8).

A remarkable rate acceleration was found when using water as solvent, most probably related to the presence of interface hydrogen bonding. The enhanced rate increase may be ascribed to the high PdNPs dispersion on functionalized SBA-15 and imposed hydrophobic interactions in the transition state. No considerable loss of activity was observed during the performance of four reuse cycles indicating the stability of the Pd/SBA-COOH catalyst for the hydrogenation of nitrobenzene.



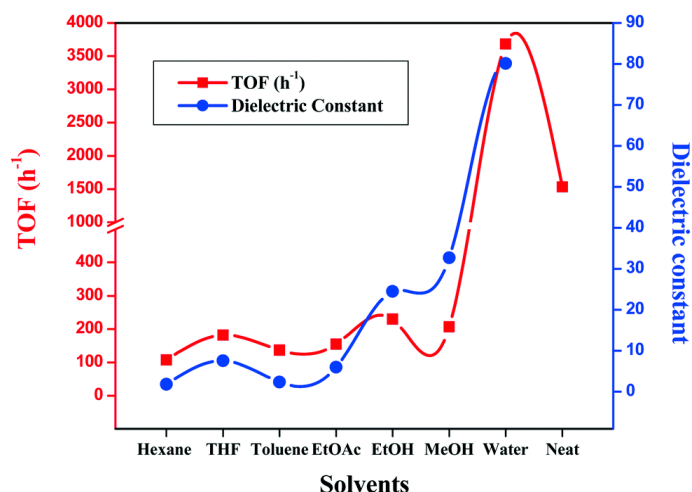


**Figure 8.** Influence of the solvent polarity on the catalytic performance for nitrobenzene hydrogenation over Pd/SBA-COOH catalyst. Reproduced with permission of Ganji et al., *New Journal of Chemistry*; published by The Royal Society of Chemistry and the Centre National de la Recherche Scientifique, 2019.

## 5. PdNPs@carbon Materials

Carbon materials encompass a myriad of nanomaterials, from activated carbon (AC), to graphite, fullerenes, carbon nanotubes (CNTs), diamond and graphene, etc., each of them presenting distinctive features [52–55], such as high surface area and porosity, tunable surface chemistry, and chemical stability. For all of this, carbon materials constitute remarkably flexible and suitable materials for numerous applications [24–28]. A large variety of carbon nanomaterials are interesting and cheaper alternatives to be used as catalysts or catalyst supports [56] in diverse reactions, improving the stability and dispersion of MNPs and, thus, enhancing their catalytic performance. As mesoporosity of the support is desirable, enabling mass transfer processes and convenient anchoring the MNPs, research has been directed at the synthesis of carbon materials with well-controlled mesoporosity. The relevance of oxygenated groups on the carbon material surface, for catalytic applications, has also led to a discerning selection of secondary treatments, such as impregnation, oxidation, and thermal treatments, for the easy tuning of the type and amount of these groups on the surface [57]. Other strategies towards catalytic performance enhancement include the incorporation of heteroatoms (N, S, B, etc.) into the carbons, which can accomplish a fine-tuning of the electronic properties of immobilized MNPs. The case of N-doped carbons has been extensively investigated, offering a very good MNPs dispersion, enhanced hydrophilicity, and additional active sites. The significantly different electronic properties of materials as CNTs and graphene, representing also very attractive catalyst supports, with numerous examples in the literature. The following examples illustrate recent advances in this field, in terms of catalytic application of carbon-derived supports for PdNPs for hydrogenation reactions. The use of graphene, CNTs, as well as biomass-derived supports for PdNPs immobilization, and the more significant factors that influence the catalytic performance is discussed.

In 2015, a new one-pot synthesis approach for the synthesis of PdNPs/reduced graphene oxide (RGO) nanocomposite materials was reported by El-Hout and co-workers [58]. Well-dispersed PdNPs on the graphene sheets were prepared through an in-situ green chemical reduction methodology. The preparation of Pd/RGO implied the sonication of GO in water, followed by addition of Pd(II) acetate to the GO suspension, and subsequent addition of a reducing agent, including oxalic acid, salicylic acid, ascorbic acid, NaOH and hydrazine hydrate, N<sub>2</sub>H<sub>4</sub> (H.H) (Figure 9). The reduction of the oxygenated functional groups and the Pd/RGO structure was corroborated by several techniques.



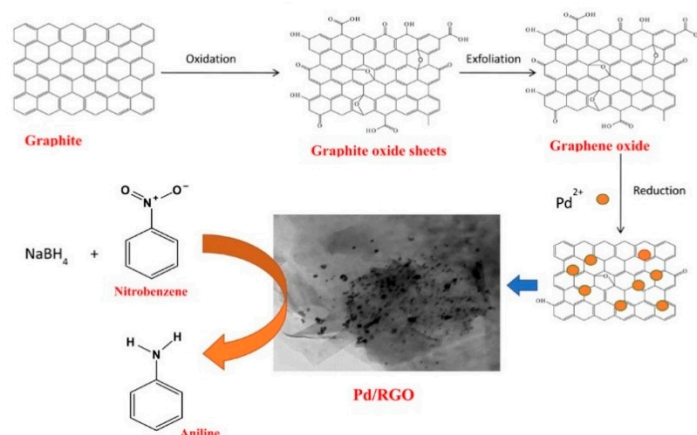


**Figure 9.** Synthetic approach for the preparation of Pd/ reduced graphene oxide (RGO), TEM image of the catalyst and application in nitrobenzene hydrogenation. Reproduced with permission from El-Hout et al., Applied Catalysis A: General; published by Elsevier B.V., 2015.

The Pd content of the catalysts was assessed by Inductively Coupled Plasma-Optical Emission Spectrometry (ICP-OES) and increases according to a reducing environment. TEM images revealed a crinkled morphology of a few ultrathin and packed graphene sheets. Well-dispersed PdNPs could be seen on the graphene sheets for Pd/RGO-salicylic acid, while other samples show less dispersed Pd particles and agglomeration. The activity of the supported PdNPs was studied for the reduction of nitrobenzene using NaBH<sub>4</sub> under mild conditions (Table 5), assessing the influence of the reduction agents used on the preparation of Pd/RGO catalysts.

**Table 5.** Catalytic results of the reduction of nitrobenzene using Pd/RGO catalyst [58].

Catalyst	Conversion (%)	Selectivity (%)	%Pd
RGO-H.H	0	0	0
Pd/C-H.H	11	30	0.64
Pd/RGO-H.H	100	100	0.49
Pd/RGO-salicylic acid	100	100	0.75
Pd/RGO-oxalic acid	100	75	0.45
Pd/RGO-NaOH	15	44	0.55
Pd/RGO-ascorbic acid	8	67	0.63

PdNPs/RGO-H.H, PdNPs/RGO-salicylic acid and PdNPs/RGO-oxalic acid catalysts showed a comparable catalytic performance, achieving complete conversion for nitrobenzene, found to be dependent on the nature of dispersed PdNPs on the graphene surface. The better results obtained for PdNPs/RGO-salicylic acid can be related to the high purity of the pristine GO support, as confirmed by TEM images, that exhibit well-dispersed PdNPs. Temperature Programmed Desorption (TPD) measurements determined the amount of active sites of PdNPs, in that PdNPs/RGO-H.H, PdNPs/RGO-salicylic acid and PdNPs/RGO-oxalic acid catalysts showed a higher number of active sites of around 9 mmol g<sup>-1</sup>, compared with ca. 6 mmol g<sup>-1</sup> for PdNPs/RGO-ascorbic acid and PdNPs/RGO-NaOH catalysts. The commercially available Pd/C-H.H compared unfavorably to the prepared PdNPs/RGO, justified by an irregular size distribution of PdNPs with agglomeration on the surface of carbon supports.

The recyclability of Pd/RGO-H.H and Pd/RGO-salicylic was investigated by the authors and is depicted in Figure 10. Both catalysts were reused for two cycles, without loss of activity.

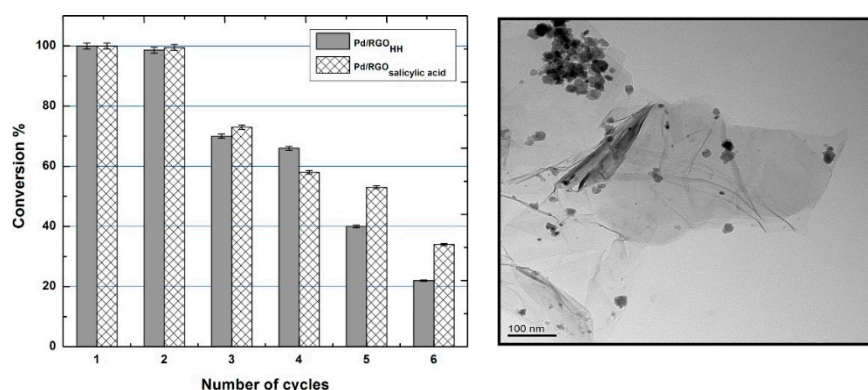


**Figure 10.** Left: recycling ability of Pd/RGO-H.H and Pd/RGO-salicylic acid catalysts in reduction of nitrobenzene. Right: TEM image of Pd/RGO-salicylic acid catalyst after the 6th run. Reproduced with permission from El-Hout et al., *Applied Catalysis A: General*; published by Elsevier B.V., 2015.

The deactivation of the Pd/RGO catalyst after the second cycle is attributed to the leaching of PdNPs, along with Pd aggregation and accumulation on the graphene surface.

In 2016, the use of reduced GO as support for PdNPs was also investigated by Nasrollahzadeh et al. The authors reported the green synthesis of PdNPs@RGO through the reduction of GO and  $\text{Pd}^{2+}$  ions using as reducing agent, barberry fruit extract [59]. The green one-step synthesis of the PdNPs/RGO consisted on the addition of the aqueous extract of *Berberis vulgaris* fruits extract [60] into prepared GO from natural graphite powder [61] followed by addition of  $\text{PdCl}_2$  under vigorous stirring, resulting in Pd(0), as monitored by Ultra Violet-Visible (UV/Vis) Spectrophotometry and Fourier Transformed Infrared (FTIR) Spectroscopy. The authors proposed a mechanism for the synthesis of the PdNPs involving the conversion of the OH functional group into the carbonyl group during a redox reaction, with reduction of Pd. The morphology of the PdNPs/RGO, as observed by Scanning Electron Microscopy (SEM), reveals that large quantities of the spherical PdNPs with an average size of about 18 nm are dispersed on the RGO surfaces (Figure 11).

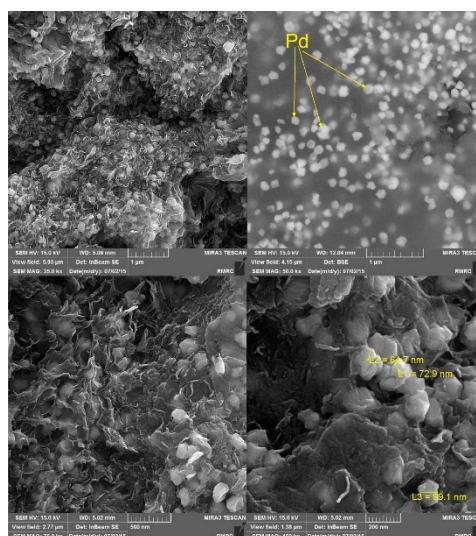


**Figure 11.** Low- and high-magnification SEM images of the PdNPs/RGO. Reproduced with permission from Nasrollahzadeh et al., *Journal of Colloid and Interface Science*; published by Elsevier Inc., 2015.

The prepared PdNPs/RGO was tested as heterogeneous catalysts for the reduction of nitroaromatic compounds by  $\text{NaBH}_4$  in an environmentally friendly medium (Figure 12). Firstly, the reduction of nitrobenzene to aniline was used to evaluate the activity of the PdNPs/RGO. High aniline yields, up to 98%, were obtained at 50 °C, with significant conversions. The authors also studied the influence of the nature of the substituents, through the reaction of different nitroarenes, reporting remarkable and robust activity, with good to excellent yields for a wide range of substrates. The gathered data showed that halogen-substituted nitroarenes were selectively reduced to their corresponding halo anilines products in high yields. Nitroarenes containing carbonyl groups also afforded very good yields of the respective products.

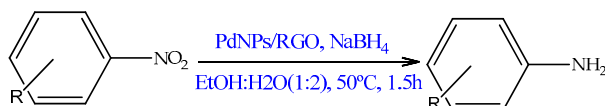


**Figure 12.** Catalytic reduction of aromatic nitroarenes over PdNPs/RGO.

In comparison with catalysts reported in the literature, PdNPs/RGO was more efficient considering the reaction time or product yields, probably due to the unique 2D structure of the RGO and the existence of the small-sized PdNPs.

The authors highlighted the importance of the RGO support towards the enhancement of the catalytic performance. Overall, the proposed method presented several advantages as high product yields, simple preparation of catalyst, simple methodology, and easy work up. The catalyst can be considered environmental-friendly, being recovered, and reused in five catalytic cycles without losing its activity [59].

Zhang and colleagues addressed the issue of stability and selectivity of Pd catalysts, reporting the design of a core-shell structure PdNPs@C supported on CNT for hydrogenation of acetylene [10]. A N-doped carbon shell was distributed on the surface of the Pd/CNT through a deposition-precipitation method. The uniformly dispersed PdNPs on the surface of the N-doped carbon shell presented an average size of ca. 1.8 nm. The ionic liquid-derived carbon covering on PdNPs was further confirmed, with a 1.5 nm carbon shell thickness on the surface of PdNPs. This microporous amorphous carbon layer could enhance mass transfer processes. The enhanced thermal stability of PdNPs was ascribed to a strong interaction among the carbon shell and PdNPs. The Pd content of Pd/CNT and Pd@C/CNT was 2.0% and 1.5%, respectively.

The selective hydrogenation of acetylene was performed to assess the catalytic performance of Pd/CNTs and Pd@C/CNTs. Pd/CNTs showed very good activity, but poor selectivity to ethylene. Although a lower catalytic activity was reported for Pd@C/CNTs, the acetylene conversion reached 100% at 150 °C (Figure 13). At lower temperatures, the low activity may be due to the carbon layer covering, while at higher temperatures the activity decrease is related to high desorption of the reactants. Nevertheless, a considerable increase in the selectivity to ethylene was observed, reaching 75% for 60% acetylene conversion, being still maintained at ca. 70%, when the acetylene conversion increased to ca. 90%.

The long-term stability of Pd@C/CNTs catalyst was examined at 140 °C, over 100 h, showing excellent stability against deactivation. The average size and pore size distribution of PdNPs of the used catalyst were similar to those of the fresh Pd@C/CNTs.

Aiming for enhanced chemical selectivity in the hydrogenation of nitro compounds, Bilgili et al. recently described the easy synthesis of a new monodisperse composite of PdNPs and GO, denoted as CPG [62]. The synthesis of CPG consisted of a mixture of  $\text{PdCl}_2$  and GO in ethanol, and further addition of a  $\text{NaBH}_4$  solution. The PdNPs were found to be homogeneously distributed over GO, presenting a mean particle size of 3.86 nm (Figure 14). XPS studies revealed the presence of metallic Pd and a small amount of Pd(II) species, the latter probably related to the oxidized species of Pd.

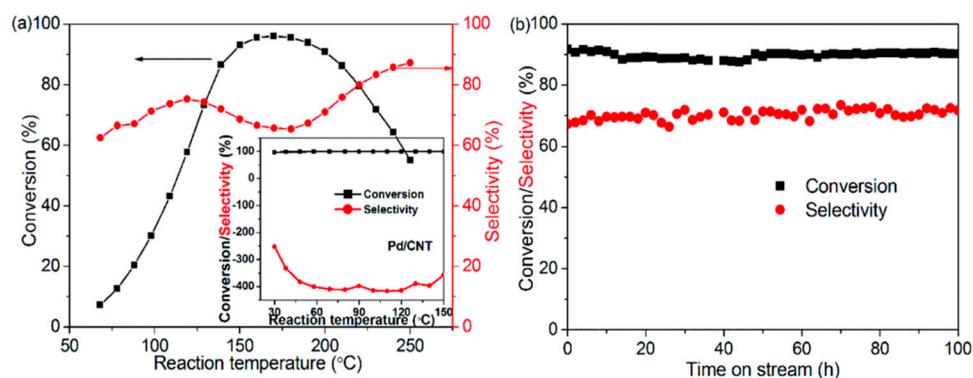


**Figure 13.** (a) Acetylene conversion and ethylene selectivity as a function of reaction temperature for Pd@C/carbon nanotubes (CNTs) and Pd/CNTs (the inset in (a)), (b) ethylene selectivity (red circles) and acetylene conversion (black squares) with time on stream for selective hydrogenation of acetylene to ethylene over Pd@C/CNTs. Reproduced with permission from Zhang et al., *Nanoscale*; published by The Royal Society of Chemistry, 2017.

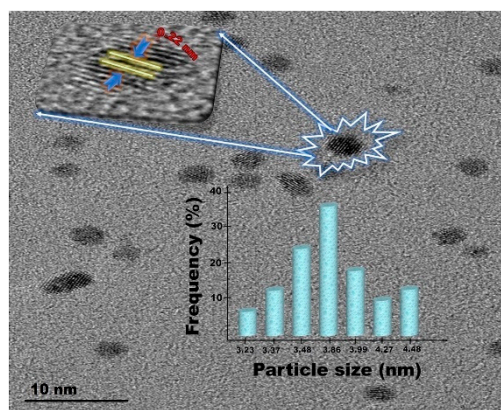


**Figure 14.** TEM, High Resolution Transmission Electron Microscopy (HRTEM) image, and particle size histogram of CPG. Reproduced with permission from Bilgili et al., *Microporous and Mesoporous Materials*; published by Elsevier Inc., 2020.

The catalytic hydrogenation of the nitroarenes was performed in the presence of  $\text{NaBH}_4$  and  $\text{N}_2\text{H}_4 \cdot \text{H}_2\text{O}$ , revealing an outstanding catalytic activity of the prepared CPG (Table 6). The catalytic performance was related to the synergistic interaction among PdNPs and the GO support material, and its ultrafine structure.

**Table 6.** Evaluation of the catalytic activity of CPG in the hydrogenation of nitrobenzene in the presence of  $\text{NaBH}_4$  [62].

<chem>c1ccccc1[N+](=O)[O-]</chem> $\xrightarrow[\text{rt}]{\text{CPG, N}_2\text{H}_4 \cdot \text{H}_2\text{O}}$ <chem>Nc1ccccc1</chem>			
$\text{N}_2\text{H}_4 \cdot \text{H}_2\text{O}$ (mmol)	Solvent	Time (h)	Conversion (%)
1.0	EtOH	8	47
2.0	EtOH	7	99
4.0	EtOH	4	>99
5.0	EtOH	4	>99
4.0	EtOH/ $\text{H}_2\text{O}$	4	>99
4.0	THF	8	>99
4.0	$\text{EtO}_2$	8	88

The catalyst was reused in several cycles, reducing selectively the nitro groups with elevated yields. The outstanding performance of the composite showed potential for further application in the reduction of nitroarenes.

In 2019, a novel halloysite-hydrochar (Hal-Char) nanocomposite was prepared by Sadjadi et al. and used as a support for PdNPs, delivering efficient catalysts for the hydrogenation reaction of nitroarenes [63]. A domestic biomass, the green head of eggplant, was chosen as the source of the hydrochar, being deposited as a layer on a halloysite via hydrothermal treatment, obtaining thus a nanocomposite, which was then employed for the immobilization of PdNPs and development of Pd@Hal-Char. The schematic procedure for the preparation of the catalysts is presented in Figure 15.

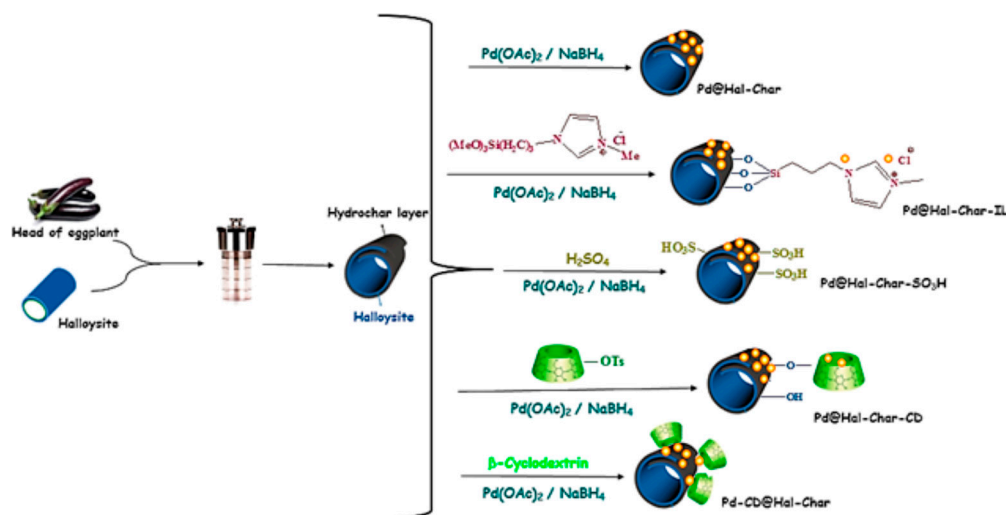


**Figure 15.** Followed approach for the synthesis of the catalysts Pd@Hal-Char. Reproduced with permission from Sadjadi et al., *ACS Sustainable Chemistry & Engineering*; published by American Chemical Society, 2019.

The textural properties of the synthesized supports were obtained from N<sub>2</sub> adsorption isotherms data, allowing to confirm the Char coverage of the Hal surface and also that the surface was covered with ionic liquid (IL) and  $\beta$ -cyclodextrin ( $\beta$ -CD). Upon Pd immobilization, a small decrease of the surface area was reported. The study of the morphology, dispersion, and average size of the PdNPs, disclosed the presence of well-dispersed PdNPs on the surface of Hal-Char without signs of aggregation, suggesting the efficiency of this material as a support. A change from the rod like structure of Hal to porous nanorods was observable.

The catalyst Pd@Hal-Char was tested towards the hydrogenation reaction of nitrobenzene and 1-nitronaphthalene, in the presence of H<sub>2</sub>, and  $\beta$ -CD, as a co-catalyst. Several control catalysts including Pd@Hal, Pd@Char, Pd@Hal-Char-CD, Pd-CD@Hal-Char, Pd@CD, Pd@Hal-Char-IL, and Pd@Hal-Char-SO<sub>3</sub>H were also prepared and tested for comparison (Table 7).

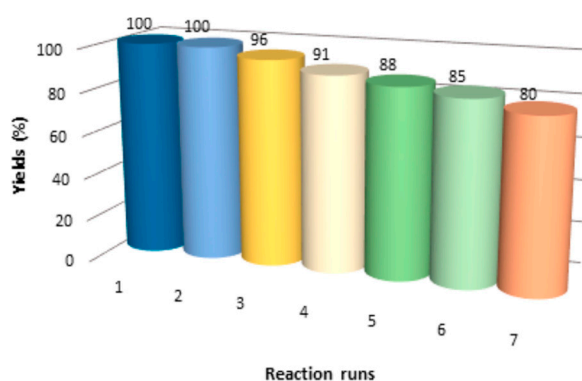
Under mild and environmentally benign conditions, moderate yields of aniline and naphthylamine were obtained after 1 h. The hydrogenation reaction at lower temperatures, with comparable yields (75% and 65% for aniline and naphthylamine) was observed with low catalyst amount and using water as solvent. The effect of Char surface modification and the role of  $\beta$ -CD on the catalytic activity were studied to clarify the role of Hal and Char. The use of  $\beta$ -CD considerably improved the yield of the reaction, acting as a phase transfer agent, being more efficient in its free form than incorporated into the framework. The authors confirmed the influence of PdNPs size and dispersion on the catalytic activity.



**Table 7.** Catalytic Activity towards aniline and naphthylamine yields and average Pd particle size of the catalysts [63].

Catalyst	Aniline Yield (%)	Naphthylamine Yield (%)	PdNPs Size (nm)
Pd@Hal	30	10	4.8
Pd@Hal+β-CD	65	60	4.8
Pd@Char	40	30	3.6
Pd@Char+β-CD	75	50	3.6
Pd@Hal-Char	75	65	3.7
Pd@Hal-Char+β-CD	100	95	3.7
Pd@Hal-Char-IL	60	30	4.5
Pd@Hal-Char-IL+β-CD	90	45	4.5
Pd@Hal-Char-SO <sub>3</sub> H	45	50	3.9
Pd@Hal-Char-SO <sub>3</sub> H+β-CD	55	55	3.9
Pd@Hal-Char-CD	60	50	4.9
Pd@Hal-Char-CD	50	40	3.8

Furthermore, the inferior catalytic activities of Pd@Hal and Pd@Char pointed out the synergy between Hal and Char. It was also found that upon IL incorporation, larger particle size and thus lower catalytic activity was obtained. The stability of Pd@Hal-Char was investigated, revealed high recyclability for this system, with the catalyst being reused in 7 runs without significantly losing its activity (Figure 16). FTIR analysis of the spent catalyst displayed the characteristic bands of the fresh Pd@Hal-Char, indicating the structural stability of the catalyst. Furthermore, no additional bands were observed for the recycled catalyst, testifying the robustness of Pd@Hal-Char catalyst.

**Figure 16.** Recyclability of Pd@Hal-Char for the hydrogenation reaction of nitrobenzene. Reproduced with permission from Sadjadi et al., *ACS Sustainable Chemistry & Engineering*; published by American Chemical Society, 2019.

Recently, Duarte et al. reported the synthesis of bio-sourced supports with enhanced catalytic properties, through an original strategy for PdNPs immobilization [64]. Size-controlled hydrochars, prepared via hydrothermal treatment, with a high degree of hydroxyl groups, from sucrose and acrylic acid sucrose-modified (10 wt.%) [65], were derivatized with ether linkers, including ammonium groups. These non-porous materials were applied as convenient supports for PdNPs through reduction of Pd(OAc)<sub>2</sub> under H<sub>2</sub> in the presence of the hydrochar (Figure 17).



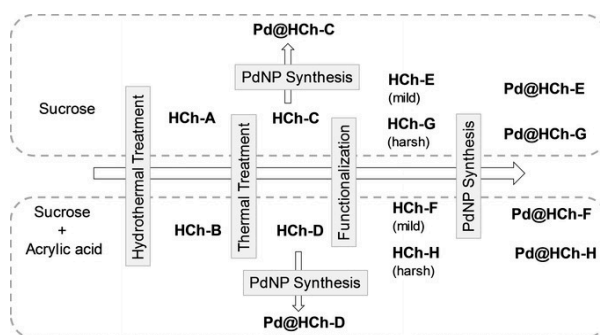


**Figure 17.** Scheme for the synthesis of functionalized hydrochars and PdNPs@hydrochars. Reproduced with permission from Duarte et al., *ChemCatChem*; published by Wiley-VCH Verlag GmbH & Co. KGaA, Weinheim, Germany, 2020.

The  $N_2$  adsorption data revealed the non-porous nature of the prepared materials. SEM images obtained before and after functionalization demonstrated the effect of the basic treatments on the morphology of the materials (Figure 18). TEM images confirmed the influence of type of support in the dispersion of PdNPs. For Pd@HCh-E, Pd@HCh-F, Pd@HCh-G, and Pd@HCh-H, the tetraalkylammonium functionalized hydrochars, PdNPs are adsorbed on the support, as a result of the interaction of the PdNPs with the ammonium groups, with no signs of agglomeration (Figure 18). The authors analyzed the effect of various parameters on the particle size of PdNPs, ranging from 5.4 to 8.0 nm. The best dispersion and smallest size for PdNPs was observed for Pd@HCh-F. XPS analysis and XRD patterns proved the presence of Pd(0).

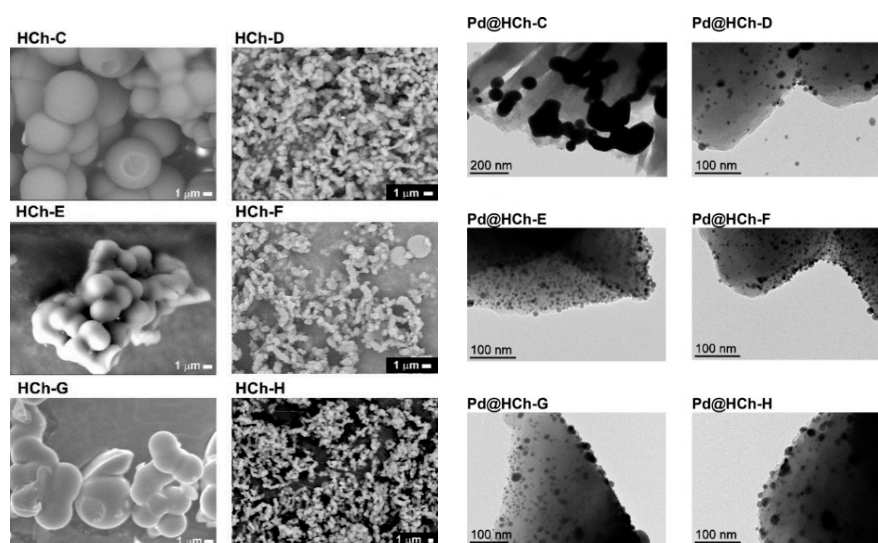
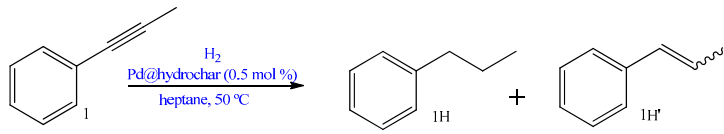


**Figure 18.** Left: SEM micrographs of thermally treated hydrochars (HCh-C and HCh-D) and their functionalization via ether linkages (HCh-E and HCh-G from HCh-C; HCh-F and HCh-H from HCh-D). Right: TEM images of hydrochar-supported PdNPs (Pd@HCh-C to Pd@HCh-H). Reproduced with permission from Duarte et al., *ChemCatChem*; published by Wiley-VCH Verlag GmbH & Co. KGaA, Weinheim, Germany, 2020.

Among the different supported PdNPs, Pd@HCh-D and Pd@HCh-F were tested as heterogeneous catalysts in the hydrogenation of 1-phenyl-1-propyne, under low  $H_2$  pressure and moderate temperature (50 °C), obtaining complete conversion in both cases, with high chemo- and stereoselectivity towards *cis*-alkene (Table 8). TEM analyses after hydrogenation showed obvious differences: while Pd@HCh-F

was not changed, Pd@HCh-D showed agglomeration. This catalytic behavior proved that the Pd surface was not passivated by the supports and favored the adsorption of alkenes.

**Table 8.** Catalytic activity of functionalized supported hydrochars PdNPs for 1-phenyl-1-propyne [64].



Catalyst	Time (h)	pH <sub>2</sub> (bar)	Conversion (%)	Selectivity (%)
Pd@HCh-D	2	3	>99	>99
Pd@HCh-F	2	3	>99	>99
Pd@HCh-D	1	1	34	91% (cis-1H') + 9% 1H
Pd@HCh-F	1	1	>99	8% trans-1H' + 72% cis-1H' + 20% 1H

Pd@HCh-F, the most active catalyst, was further investigated for the hydrogenation of alkynes, alkenes, and carbonyl and nitro derivatives, exhibiting high yields of 85–95% in all cases [64]. Moreover, the use of this catalyst avoided the use of expensive reagents and high temperatures, leading to improved yields in shorter reaction times. The superior recyclability of Pd@HCh-F was proven, through the reuse in 10 consecutive runs with preserved catalytic reactivity in accordance with the unchanged catalytic materials as assessed by TEM, with no detectable metal. Conversely, the activity of the commercial catalyst Pd/C dropped after three cycles, reaching only 36% conversion in the subsequent run. In general, the non-porous character of HCh-D and derived hydrochars was beneficial against detrimental diffusion paths throughout the support, allowing softer reaction conditions [66,67].

## 6. PdNPs@zeolites

Zeolites are crystalline materials widely used in several fields, as adsorption, separation processes, and also heterogeneous catalysis [26,68,69]. The unique features of these materials including high porosity, intrinsic acidity, shape selectivity, mechanical stability, exchange capacity makes them particularly appealing as hosts for encapsulation of PdNPs. Nevertheless, their essentially microporosity character can pose as a disadvantage, owing to diffusion limitations. For this reason, the widespread use of zeolites as catalytic supports is limited, when compared with mesoporous materials. In these cases, the immobilization is somewhat limited to the external surface.

To face this drawback, quite a few approaches have been endeavored towards accessibility and mass transfer enhancement for these materials [70,71]. These methods aim for the development of hierarchical zeolites, presenting micro and mesoporosity, which efficiently combine the inherent zeolites properties with mesoporosity. For this matter, post-synthesis treatments, which result on enlargement of the existent microporosity and generation of mesoporosity, can be applied [71–74]. The number of publications regarding potential applications of hierarchical zeolites has increased [71,72,75], although their use as supports for PdNPs for hydrogenation reactions is somewhat less described.

In 2016, Wang et al. reported the in-situ (IS) synthesis of a Pd/ZSM-5-IS catalyst based on an azeotropic distillation process combined with a solvothermal method [76]. The synthesis involved the generation of a reverse microemulsion in the presence of a surfactant, controlled the crystal growth process and stability of the nanoparticles (Figure 19). The resulting emulsion was treated by an azeotropic distillation, and carbon coated PdO NPs were formed after a solvothermal process and carbonization. These PdO NPs were mixed into the ZSM-5 through a solvothermal process, and uniform-sized and non-aggregated PdNPs confined within ZSM-5 structure were achieved after calcination and reduction. The Pd loading of the catalysts was about 1.8 wt%, as determined by ICP-OES. XRD patterns confirmed a high degree of crystallinity and the presence of metallic Pd for the Pd/ZSM-5-IS samples.

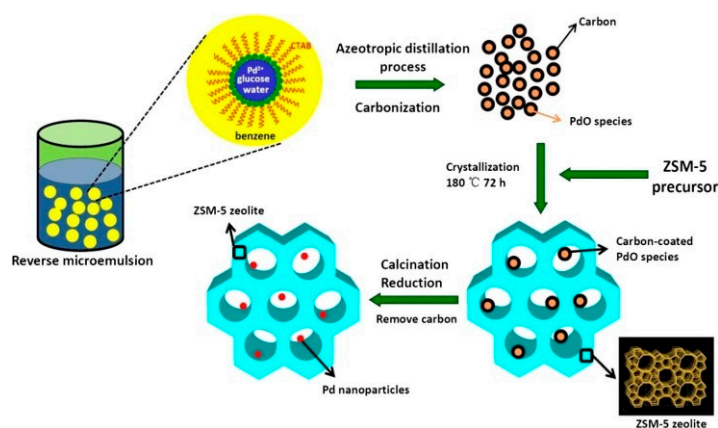


**Figure 19.** Procedure of the preparation of Pd/ZSM-5-IS catalyst. Reproduced with permission from Ma et al., *Chemical Engineering Journal*; published by Elsevier B.V., 2015.

The confinement within ZSM-5 prevented the sintering and aggregation of PdNPs and provided high thermal stability. PdNPs were highly dispersed, uniform in size and with a small average particle size (3.8 nm) and a narrow size distribution. The evidences point out the PdNPs incorporation into the intracrystalline structure of ZSM-5 zeolite, constrained by the rigid zeolitic framework, yielding Pd/ZSM-5-IS. When compared to conventional ZSM-5, Pd/ZSM-5-IS displays mesoporosity, with a narrow pore size distribution and centered at 1.5 nm and 4 nm. XPS measurements of the Pd/ZSM-5-IS sample confirmed the complete reduction of PdO to Pd(0). For comparison purposes, Pd/ZSM-5 was also prepared through a conventional method, denoted as Pd/ZSM-5-IM.

The catalytic activity of Pd/ZSM-5-IS and Pd/ZSM-5-IM towards the hydrogenation of *p*-nitrophenol to *p*-aminophenol were scrutinized (Figure 20). Although Pd/ZSM-5-IM showed a quite similar catalytic activity to Pd/ZSM-5-IS at 80 °C, the temperature increase to 100 °C led to a significant difference between the two. Conversion of *p*-nitrophenol for Pd/ZSM-5-IM was only 75% while a complete conversion was accomplished for Pd/ZSM-5-IS, most probably attributed to the leaching and aggregation of the active species with an increase in the reaction temperature in this case, as the majority of PdNPs are located on the external surface of ZSM-5. The authors point out the thermal and chemical stability of the active sites, the small size of PdNPs as key factors for the enhanced catalytic activity for Pd/ZSM-5-IM.

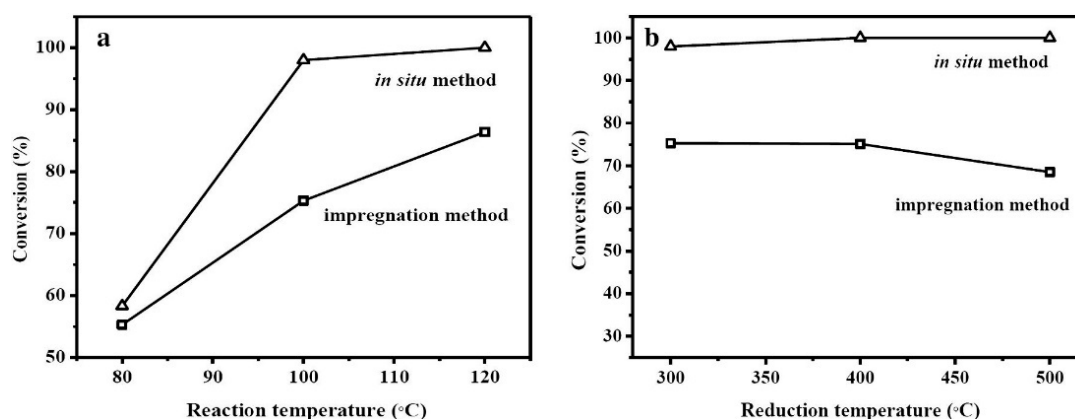


**Figure 20.** (a) Influence of the reaction temperature and (b) Influence of the reduction temperature on the conversion of *p*-nitrophenol catalyzed by Pd/ZSM-5-IS and Pd/ZSM-5-IM. Reproduced with permission from Ma et al., *Chemical Engineering Journal*; published by Elsevier B.V., 2015.

The recyclability of both catalysts was studied, assessing possible deactivation and the number of catalytic cycles. Pd/ZSM-5-IS presented an outstanding recycling stability, while Pd/ZSM-5-IM showed 65% of deactivation after five consecutive runs. After five cycles of reuse and compared with the fresh catalyst, particle size and crystallinity of the spent Pd/ZSM-5-IS remains unchanged. The confinement of PdNPs within the structure of ZSM-5 also provided efficient protection against contact of the catalyst with toxic impurities. The performance of Pd/ZSM-5-IS catalyst also compared favorably with Pd catalysts reported in the literature, as Pd-B/TiO<sub>2</sub> [77], Pd/Al<sub>2</sub>O<sub>3</sub> catalyst [78], and so on.

In 2016, Cui et al. reported the synthesis of Pd/zeolite hybrids with encapsulated PdNPs inside mesoporous silicalite-1 nanocrystals (Pd@mnc-S1) by a simple one-pot method [79] from silica nanoparticles and chloropalladic acid (Figure 21) [80], ensuring the complete incorporation of PdNPs inside mesoporous silicalite-1 nanocrystals. Further aggregation was prevented using a small amount of polyvinylpyrrolidone (PVP). The resulting amorphous silica aerogel was further heated at 120 °C in an autoclave with a limited amount of water to trigger the Kirkendall growth of mesoporous silicalite-1 nanocrystals. Consecutive calcination of the obtained solid was performed for the removal of all organic components and reduction of PdNPs to the metallic state.

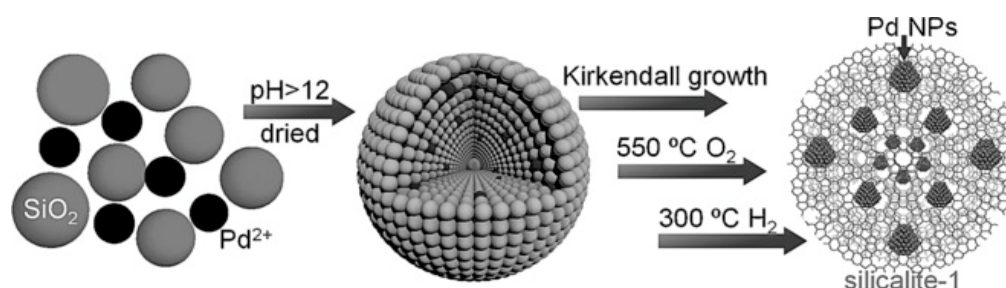


**Figure 21.** Schematic procedure for Pd@mnc-S1. Reproduced with permission from Cui et al., *Angewandte Chemie—International Edition*; published by Wiley-VCH Verlag GmbH & Co. KGaA, Weinheim, Germany, 2016.

TEM and SEM images show the formation of 200 nm silicalite NPs. High Resolution Transmission Electron Microscopy (HRTEM) revealed the high crystallinity of the silicalite-1 nanocrystal, as confirmed by XRD, as well as the formation of metallic PdNPs. The encapsulation of PdNPs did not affect the crystallinity and mesoporous structure of the silicalite-1 nanocrystals. Elemental mapping images revealed the homogeneous distribution of PdNPs in the silicalite-1 nanocrystals with an estimated Pd content of 1.7 wt%. The catalyst presented a high thermal stability, confirming the integration of PdNPs within the framework of silicalite-1 nanocrystals. PdNPs on the surface of the control sample Pd/silicalite-1 showed significant aggregation with a significant particle size increase after the calcination process.

The hydrogenation of nitrobenzene progressed effectively over Pd@mnc-S1 due to its integrated structure and efficient mass transfer through the microporosity of MFI zeolite. Remarkably, Pd@mnc-S1 delivered 87% of product conversion within 2 min, comparable to the conversion (98%) over Pd/C. The deposited PdNPs did not block the porosity of silicalite-1 and more significantly, the mesopores and nanometric size of the zeolite nanocrystals abbreviated the mass transfer pathway of substrates to the PdNPs inside Pd@mnc-S1. This has considerably enhanced the reaction rate, offering a comparable catalytic activity of Pd@mnc-S1 to uncovered PdNPs. The Pd@mnc-S1 acted as a reusable heterogeneous catalyst, with excellent stability.

The molecule-size dependent selectivity of Pd@mnc-S1 was tested in the same conditions (Figure 22). The use of the commercial Pd/C with PdNPs accessible to all species, led to the hydrogenation of nearly all nitroarenes, independently of their molecule dimensions. Overall shape-selectivity owing to the mesoporosity as well as the nanosized crystals of the catalyst support promoted mass transfer to PdNPs and their catalytic performance.



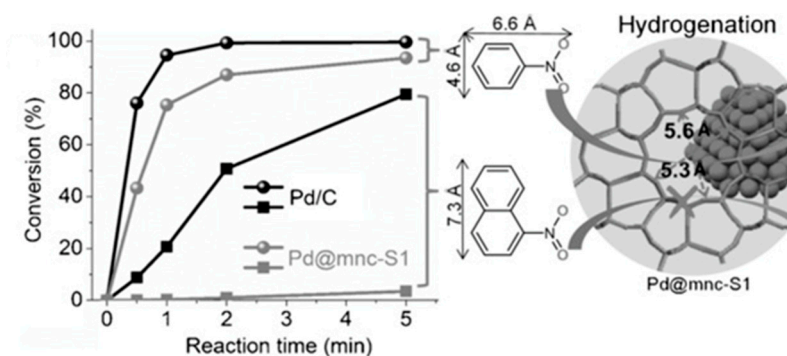


**Figure 22.** Hydrogenation reactions over Pd@mnc-S1 or Pd/C. Reproduced with permission from Cui et al., *Angewandte Chemie—International Edition*; published by Wiley-VCH Verlag GmbH & Co. KGaA, Weinheim, Germany, 2016.

In 2017, Zhang and co-authors reported a new approach aiming to enhance the selectivity of PdNPs in the hydrogenation reaction of substituted nitroarenes, over the preparation of a core-shell Pd@Beta catalyst, showing advantages originated from the synergy between the high catalytic activities of PdNPs, and the selective adsorption of reactants on the microporosity of zeolites.

The synthesis of Pd@Beta was accomplished by a seed-directed route of zeolite Beta crystals proceeding by a core-shell growth mechanism that led to the development of newly formed zeolite from the containing PdNPs. The purity of Pd@Beta was confirmed by XRD and N<sub>2</sub> adsorption isotherms. SEM and Scanning Transmission Electron Microscopy (STEM) provided evidence for the uniform morphology of PdNPs@Beta and for the location of PdNPs within Pd@Beta [67] (Figure 23, left). The Energy-Dispersive X-ray Spectroscopy (EDS) analysis corroborated the core-shell growth, showing the full encapsulation of the PdNPs. The images further show highly dispersed PdNPs within the zeolite crystals, with diameters of 0.9–3.1 nm.

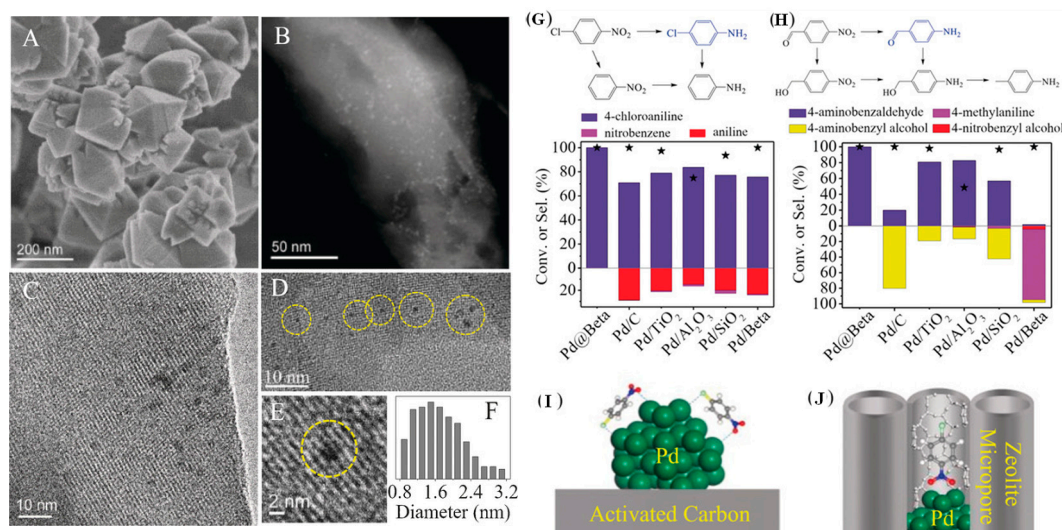


**Figure 23.** Left: (A) SEM, (B) STEM, and (C–E) HRTEM images of Pd@Beta. PdNPs are highlighted in yellow. (F) Size distribution of the PdNPs. Right: Substrate conversions (N) and product selectivities (colored columns) for the hydrogenation of (G) 4-nitrochlorobenzene and (H) 4-nitrobenzaldehyde on various catalysts. Proposed models for the 4-nitrochlorobenzene adsorption on (I) Pd/C and (J) Pd@Beta. Color code: C gray, Cl light green, H white, N blue, O red, Pd dark green. Reproduced with permission from Zhang et al., *Angewandte Chemie—International Edition*; published by Elsevier B.V., 2017.

The hydrogenation of 4-nitrochlorobenzene was studied as a model reaction in the presence of various Pd-containing catalysts (Figure 23, right). PdNPs@Beta provided high activity and selectivity obtaining 4-chloroaniline as the exclusive detectable product, ascribed to the steric effects on the adsorption of the nitroarenes onto the zeolite microporosity. On the other hand, conventional Pd catalysts lacked stability and selectivity. These results point out that the reduction of nitro groups over chloro groups is favored by Pd@Beta. The reason for this high selectivity must be related to the encapsulation of PdNPs, and not to its size, as suggested by the authors. To compare the adsorption selectivities and strengths for nitrobenzene and chlorobenzene on the Pd catalysts, adsorption replacement studies were conducted. Nitrobenzene was significantly more strongly adsorbed on Pd@Beta in comparison to chlorobenzene. The authors assumed that the zeolite cover has an influence on the accessible Pd surface.

The adsorption of 4-nitrochlorobenzene on Pd@Beta leads to a parallel alignment of the molecule regarding the microporous channels, and to the favored bonding to the Pd sites through the nitro group. Pd@Beta showed high stability in recycling tests, without Pd aggregation or leaching, with a superior performance than the commercial Pd/C catalyst. The obtained data verified the overall application of Pd@Beta for the selective hydrogenation of nitroarenes.

Wang and colleagues reported the selective hydrogenation of furfural over Pd@S-1-OH catalysts originated from the fixation of PdNPs inside of silicalite-1 zeolite, through the silanol groups mediated functionalization of the zeolite host (Figure 24) [81]. The -OH modified S-1 was prepared using as precursors diethoxydimethylsilane (DEMS) and tetraethyl orthosilicate, obtaining S-1-OH<sub>x</sub> (x = molar % of DEMS in the total amount of silica of the starting solution). For the synthesis of Pd/S-1-OH, S-1-OH-10 zeolites were added into an aqueous Na<sub>2</sub>PdCl<sub>4</sub> solution followed by ultrasonic treatment. Pd/S-1-OH-10 seeds were obtained after calcination and reduction. The Pd/S-1 seeds were attained through the same method, using S-1 zeolite. For the synthesis of Pd@S-1-OH-10, Pd/S-1-OH-10 seeds, SiO<sub>2</sub>-Me and TPAOH were mixed and grinded and thermally treated. After the removal of the organic template and calcination of the silanol groups, Pd@S-1-OH-10 was obtained. The procedures for the preparation of the materials are shown in Figure 24. Pd@S-1 synthesis followed the same procedure, with Pd/S-1 and pure silica. Pd@S-1-OH-10 was additionally treated with HF.

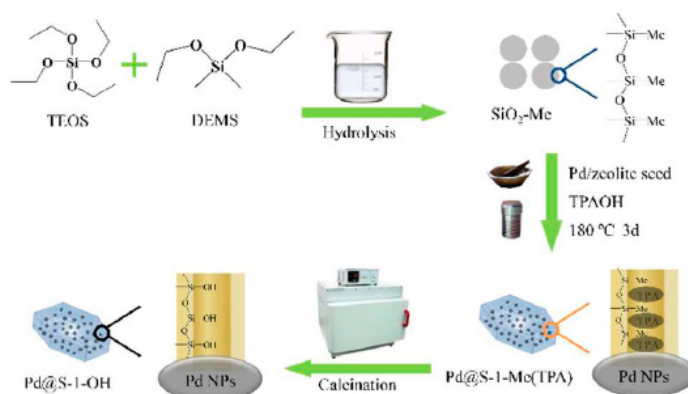


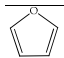
**Figure 24.** Experimental approach for the preparation of Pd@S-1-OH. Reproduced with permission from Wang et al., *ACS Catalysis*; published by American Chemical Society, 2017.

XRD patterns of S-1, Pd@S-1-OH-10, and Pd@S-1-OH-20 samples revealed the typical peaks assigned to the MFI structure. Samples S-1, Pd@S-1-OH-10, and Pd@S-1-OH-20 presented high textural parameters, almost unaffected by inner surface modification. Comparable Pd loading amounts were determined for Pd@S-1-OH-x (0.34 wt%), Pd/S-1, and Pd/Al<sub>2</sub>O<sub>3</sub> (0.33 wt%). More hydrophilic surfaces were observed for Pd@S-1-OH-10 and Pd@S-1-OH-20. The TEM images of Pd@S-1-OH-10 NPs confirmed the fixation of these particles within the S-1 crystals and also a PdNPs size distribution in Pd@S-1-OH-10 and Pd@S-1 that falls within the range 3–11 and 5–11 nm, respectively. The PdNPs are



located on the outer surface of S-1 zeolite on Pd/S-1, presenting a size distribution at 4–10 nm. Hydrogenation of furfural was studied to assess the catalyst activity. The reaction involves different pathways, yielding products as furfuryl alcohol, furan, dihydrofuran, tetrahydrofuran, tetrahydrofurfuryl alcohol, and bulky ether molecules. Furfural conversion and furan selectivity for Pd@S-1-OH-10 significantly enhanced when the temperature is increased to 275 °C (Table 9). Lower furfural conversions were obtained in all cases for the Pd@S-1 catalyst. The best catalytic result over Pd@S-1 was obtained at 250 °C, with a furfural conversion of 93% and furan selectivity at 97%. The Pd/S-1 displayed low furan selectivities, lower than 13% (not shown). The gathered data highlight the remarkable catalytic performance of Pd@S-1-OH-10, even when compared to that reported for the industrial catalyst, Pd/Al<sub>2</sub>O<sub>3</sub> [82]. In addition, the larger molecules arising from furfural the condensation were observed as main products over Pd/S-1 and Pd/Al<sub>2</sub>O<sub>3</sub>, however not detectable for Pd@S-1-OH-10 and Pd@S-1. Since the Pd sites of Pd@S-1-OH-10 and Pd@S-1 are fixed in zeolite crystals, bulkier molecules are unlikely to form, given the micropores dimensions. This enhanced catalytic performance of Pd@S-1-OH-10 is fairly attributed to its more hydrophilic zeolite sheath. Pd@S-1-OH-20 has shown lower furan selectivities, which might be related to its lower crystallinity, and consequently a reduced micropore volume and surface area.

**Table 9.** Catalytic results for furfural hydrogenation over Pd@S-1-OH-10 and Pd@S-1 [81].

Catalyst	Temperature (°C)	Conversion (%)	Selectivity (%) 
Pd@S-1-OH-10	150	56.7	82.5
	175	89.5	89.7
	200	>99.9	95.9
	225	>99.9	98.4
	250	>99.9	>99.9
	275	>99.9	>99.9
Pd@S-1	150	48.9	85.0
	175	62.8	91.4
	200	86.6	92.8
	225	91.3	93.2
	250	92.9	97.1
	275	86.6	82.6

To unveil the significance of the hydrophilic zeolite sheath, Pd@S-1-OH-10 was treated with HF to partly destroy the zeolite sheath. Pd@S-1-OH-10-HF exhibited a significant reduction of furfural conversion (80%) and furan selectivity (58%), proving the key role of S-1-OH zeolite sheath in catalytic furfural hydrogenation. To assess catalyst stability, the catalytic performance of Pd@S-1-OH-10 was investigated over time at 200 °C. While selectivity was maintained, a conversion drop is observed, being restored to >99.9% upon calcination. Deactivation of the catalyst was related to coke formation. TEM images of the used Pd@S-1-OH-10 catalyst still exhibit a very similar PdNPs diameter distribution to that of the fresh catalyst, along with negligible Pd leaching, highlighting the stability of the zeolite sheath.

In 2018, Zhao and co-workers described a strategy synthesis for encapsulated PdNPs inside FER zeolite through a layer reassembling procedure [83]. Pd precursor incorporation was achieved by swelling FER layers in RUB-36 using cetyltrimethylammonium cations (CTA<sup>+</sup>) followed by a subsequent ion exchange process, excluding the organic template diethyldimethyl ammonium (DEDMA) (Figure 25). The removal of the long CTA<sup>+</sup> chain allowed the recovery of the distances between FER layers. The condensation of silanol groups and PdNPs establishment amongst the adjacent FER layers was finally completed after calcination and reduction.

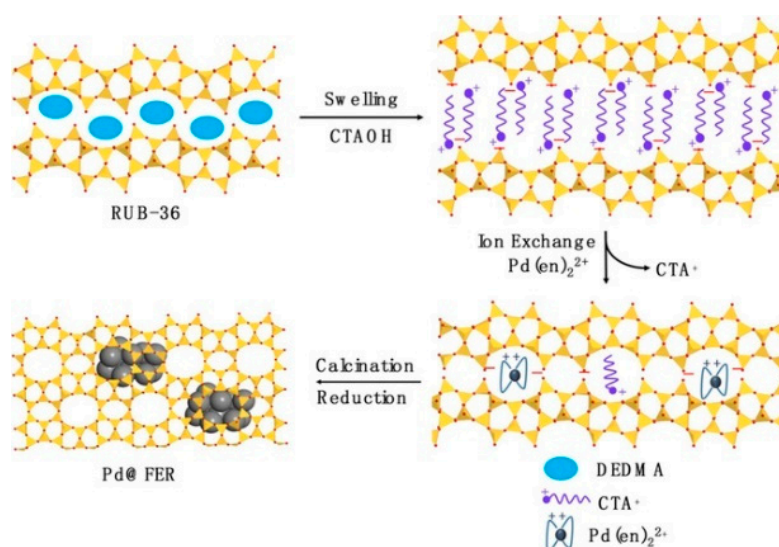


**Figure 25.** Procedure for the encapsulation of PdNPs in FER zeolite. Reproduced with permission from Zhao et al., *ChemCatChem*; published by Wiley-VCH Verlag GmbH & Co. KGaA, Weinheim, Germany, 2018.

XRD patterns confirmed the swelling between FER layers, distant enough to offer space for the access of  $\text{Pd}(\text{en})_2^{2+}$ , and high crystallinity for Pd@FER. The authors validated the successful Pd introduction (1.4 wt%) in-between FER layers. Typical flake morphologies were observed in SEM images of Pd@FER, quite like Pd/RUB-37 synthesized through an incipient wetness approach, with 0.9 wt% Pd content. TEM images point out well-dispersed and ultrafine 1.4 nm PdNPs in the zeolite, and only slight sintering near the edges of the sheets. Pd/RUB-37 shows 4.2 nm PdNPs with a broader size distribution. The  $^{29}\text{Si}$  MAS NMR spectrum of Pd@FER indicates a considerable number of SiOH groups on the support. The homogeneous distribution of PdNPs within FER zeolite may result from its distinctive 2D structure. Particle sintering among different layers is hindered, as Pd precursors or NPs are in between the FER layers with no micropores; therefore, enhancing thermal stability. The chemical state of PdNPs was studied by XPS, revealing metallic Pd for both samples, with an intensity of the signal considerably higher for Pd/RUB-37, as in this case most of PdNPs are located on the surface.

Hydrogenation reactions of 1-hexene and 1-phenyl-1-cyclohexene with different steric hindrance were performed with the catalysts. Pd@FER showed a somewhat lower reaction rate, and 100% conversion of 1-hexene, given its molecular size close to the pore aperture of FER zeolite. On the other hand, when 1-phenyl-1-cyclohexene, a molecule with a much larger steric hindrance was used as substrate, almost no conversion is seen for Pd@FER catalyst, while for Pd/RUB-37, a conversion of 30% is obtained. In the case of 1-hexene hydrogenation reaction, a considerable amount of 2-hexene is observed for both catalysts with substantially slower conversion for Pd@FER due to the same reason (Figure 26).

Furthermore, Pd@FER has shown high activity for benzaldehyde with 100% to toluene, whereas Pd/RUB-37 presented lower benzaldehyde conversion, and a significant amount of benzyl alcohol was observed, reaching no more than 66% of toluene yield. Conversely, Pd/RUB-37 has shown very high activity for the significantly larger diphenylmethanone, with 100% transformation into diphenylmethane after 60 min. Pd@FER reached no more than 10% of diphenylmethanone yield given the steric hindrance. Overall, these results unequivocally validate the shape-dependent selectivity of Pd@FER for hydrogenation reactions and prove the successful encapsulation of PdNPs.

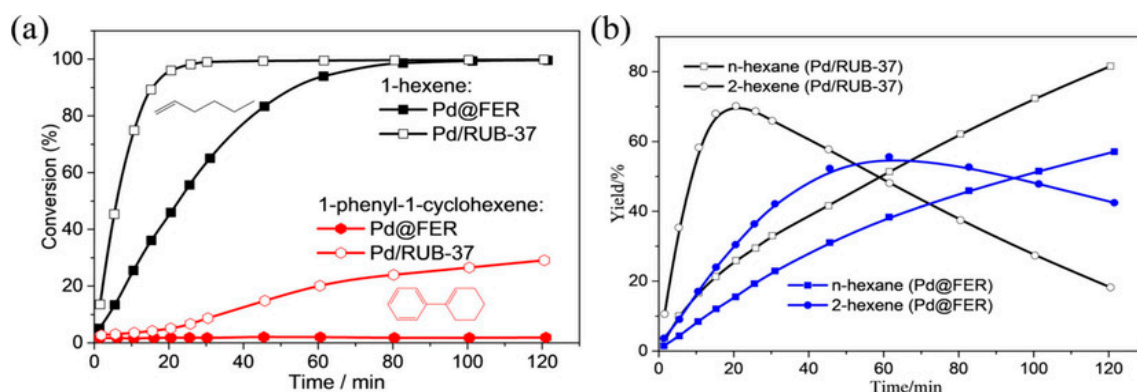


**Figure 26.** (a) Hydrogenation activities of 1-hexene and 1-phenyl-1-cyclohexene; (b) product distributions for 1-hexene hydrogenation over Pd@FER and Pd/RUB-37 catalysts. Reproduced with permission from Zhao et al., *ChemCatChem*; published by Wiley-VCH Verlag GmbH & Co. KGaA, Weinheim, Germany, 2018.

Zhang et al. also investigated the influence of electronic and steric effects in the hydrogenation of nitroarenes over Pd@Beta and Pd@MWW catalysts [84] (Figure 27). Pd@zeolite samples were prepared by a one-pot synthesis using an  $\text{Pd}(\text{NH}_3)_4(\text{NO}_3)_2$  aqueous solution and subsequent reduction [28,85,86]. The introduction of the Pd caused no significant structural or textural changes on the zeolites.

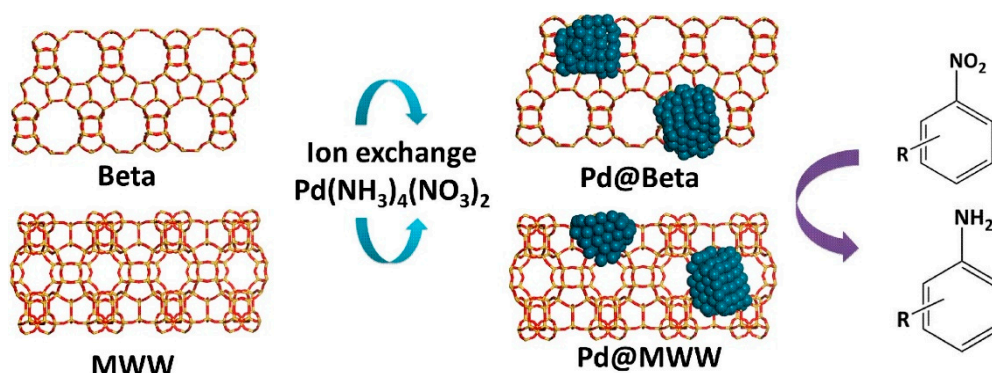


**Figure 27.** Proposed approach towards preparation and application of Pd@Beta and Pd@MWW. Reproduced with permission from Zhang et al., *Catalysis Today*; published by Elsevier B.V., 2019.

Slightly lower surface areas and a micropore volume decrease was observed for Pd@zeolite in regard to the parent material, likely due to a partial blockage of the porosity of the zeolites. TEM images proved the presence of uniformly distributed PdNPs in Beta and MWW zeolites, presenting an average particle size of 2.6 and 1.7 nm in accordance with the different dimensions of their channels diameter, 0.59 nm for Beta and 0.49 nm for MWW zeolite. A Pd content of 0.38 and 0.36 wt%, was estimated for Pd@Beta and Pd@MWW, respectively. The FTIR spectra taken after exposure of Pd@Beta and Pd@MWW catalysts to CO atmosphere revealed that that  $\text{Pd}^{\text{n+}}$  species were easier to reduce when supported on Beta zeolite.

The catalysts were applied to the hydrogenation of nitroarenes, showing activity for most of the investigated substrates, yielding the aromatic amines without the detection of by-products. Pd@Beta catalyst showed a higher catalytic performance than Pd@MWW, even though they present similar Pd contents (0.38 wt% for Beta and 0.36 wt% for MWW) and average size of PdNPs. The lower catalytic activity of Pd@MWW is most likely related to diffusional constraints of the MWW microporosity. A better performance was observed for Pd@Beta given its large microporosity, facilitating mass transport of the molecules. To explore the electronic effect, electron-donating and

electron-withdrawing substituents in meta-position on the aromatic ring were selected to investigate details of the hydrogenation of nitroarenes (Figure 28). The gathered data show that steric effects are critical for the reaction rate of nitroarenes, in regard to both molecular sieving effect of the zeolite and hindrance of the groups. The reduction of the substituent groups on the ortho position is more difficult than the meta- and para- isomers.

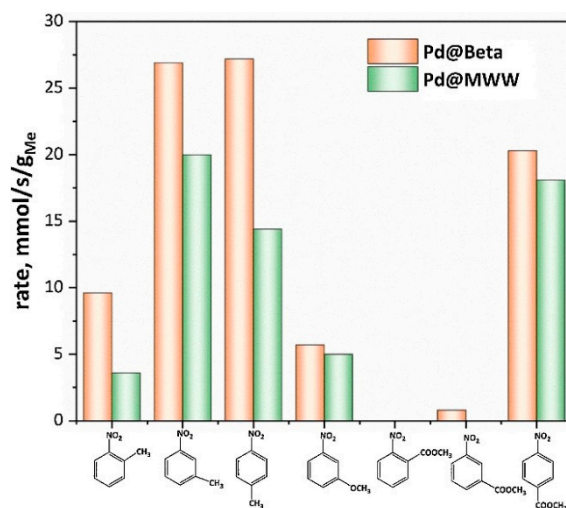


**Figure 28.** Initial reaction rates for the hydrogenation of nitroarenes over Pd@Beta and Pd@MWW. Reproduced with permission from Zhang et al., *Catalysis Today*; published by Elsevier B.V., 2019.

The reusability of Pd@Beta was investigated, performing the hydrogenation of 3-nitrotoluene with the reuse of Pd@Beta up to five cycles. The authors observed high conversions in three cycles, with high selectivity to m-toluidine. Upon the fourth and fifth runs, a conversion drop was observed and the spent Pd@Beta catalyst was regenerated and reused for two further cycles, recovering almost a full conversion, with constant selectivity. The deactivation of Pd@Beta was mainly assigned to contamination or coke formation on PdNPs.

## 7. PdNPs@MOFs

MOFs are hybrid crystalline porous materials, featuring periodic network structures, consisting in the assembly of metal ions/clusters and organic linkers [23,87]. MOFs are very promising materials for application in a variety of fields, with a special focus on catalysis, one of its most rapidly growing field of application. The intrinsic properties of MOFs involve highly porous structures with well-dispersed active sites, which significantly facilitate the access of reactants and a stable character, ensuring recyclability. In addition, their highly uniform pore shapes and sizes confers MOFs its size-selective catalytic properties.

MOFs are therefore exceptional supports for PdNPs, offering a diversity of functionalized MOFs skeleton, and allowing the catalyst separation and reuse [24,88]. For PdNPs@MOF systems, PdNPs act as active centers and MOFs as stabilizers, the simplest type of synergy between both. Four synthetic approaches are usually considered for the immobilization of PdNPs on MOFs: (1) in the structure and/or on the external surface of the MOF, prior to MOFs synthesis; (2) introduction of the MNPs into the reaction solution for MOF growth, incorporating PdNPs; (3) step-by-step synthesis of MNPs@MOF; (4) synthesis of MNP@MOF in one-step. Through the synergy between PdNPs and MOFs, enhanced catalytic activity can be achieved. The research advances of Pd@MOFs in heterogeneous catalysis for hydrogenation reactions are discussed below, highlighting the key factors contributing to the catalytic performance of these systems.

Zhang et al. studied the hydrophilicity/hydrophobicity of two MOFs, MIL-101, and MIL-53 on encapsulated PdNPs and the resulting catalytic activity towards phenol hydrogenation (Figure 29) [89].



MIL-101 and MIL-53 were obtained following procedures described in the literature [90,91] and Pd@MOFs catalysts via a deposition-reduction methodology. Given the high hydrophilicity of mesoporous MIL-101, it performed better as a support for small PdNPs (2.3 nm), most likely related to weak  $\pi$  interaction, that provided high dispersion of the Pd precursor. On the other hand, larger sized PdNPs (4.3 nm) were found on the surface of the microporous hydrophobic MIL-53, with clear signs of aggregation. XRD patterns suggested a finely dispersion of the PdNPs for both materials. The Pd dispersion achieved for Pd/MIL-101 and Pd/MIL-53 was of 44% and 35%, correspondingly. Surface hydrophobicity was assessed by phenol and cyclohexanone adsorption studies on MILs. Stronger phenol adsorption was observed for MIL-53, as a result of the narrower porosity of this material that can lead to a stronger hydrophobic section in its pores.

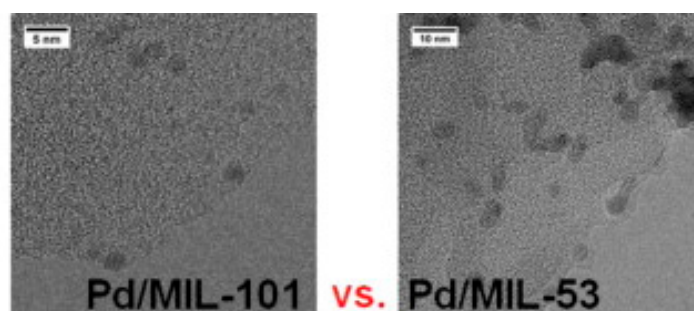


**Figure 29.** TEM images of the Pd@MOFs applied towards phenol hydrogenation. Reproduced with permission from Zhang et al., *Catalysis Communications*; published by Elsevier B.V., 2013.

The catalytic activity of Pd/MIL-101 and Pd/MIL-53 for phenol hydrogenation has shown selectivities >98% for cyclohexanone, given its stronger adsorption affinity for both MILs. The performance of Pd/MIL-101 was always better than Pd/MIL-53. The hydrogenation of the phenyl group compounds most probably occurs on the Pd surface, as reported in the literature [92]. The mesoporosity and hydrophilicity of MIL-101, as well as the smaller particle size for PdNPs, are pointed out as responsible for its higher catalytic activity, as some PdNPs may exist inside its porosity, originating metal- $\pi$  interactions between the framework and the particles. The catalysts were recycled up to 5 times without Pd leaching to the solution. Nevertheless, a decrease in the activity was detected after three runs, related to particle size growth in both cases, increasing to 4.1 and 5.3 nm, for Pd/MIL-101, and Pd/MIL-53, respectively, as reported in previous studies [93,94]. Particle aggregation was also considered accountable for catalyst deactivation.

Xu and co-workers also used MIL-100 to synthesize a PdNPs@MIL-100(Fe) composite to be applied as catalyst for 2/3/4-nitrophenol reduction [95]. MIL-100(Fe) nanospheres were obtained through a modified procedure according to previous works [96]. The Pd@MIL-100(Fe) composite was prepared by encapsulation of PdNPs on MIL-100(Fe) nanospheres, according to a solution impregnation approach followed by a hydrogen-reduction method. TEM images of MIL-100(Fe) showed particles with a spherical morphology with ca. 120 nm, assembled by aggregation of MIL-100(Fe) NP preferentially along a particular lattice plane (Figure 30, left).

The confinement effect within MIL-100(Fe) allowed to obtain small and highly stable PdNPs (4–6 nm) as well as highly dispersed on the external surface and in the porous network. The amount of Pd on the composite was 1.57 wt%. MIL-100(Fe), as determined by ICP. PdNPs@MIL-100(Fe) displayed similar type I adsorption isotherms, revealing their microporous structure. The appreciable decrease of surface area observed for Pd@MIL-100(Fe) indicates a partial occupation of the porosity of the framework by PdNPs formed within this structure. XPS spectra confirmed that most of the Pd is in the reduced form.

The catalytic activity towards nitrophenol reduction to aminophenol by  $\text{NaBH}_4$ , for Pd@MIL-100(Fe) nanocomposite was studied, revealing conversion ratios of about 100%, 97%,

and 92%) for 4-nitrophenol, 2-nitrophenol, and 3-nitrophenol, respectively, related to electronic density of the nitro groups. Additionally, conjugation and inductive effects are present for 2-nitrophenol and 4-nitrophenol. The high performance stability of Pd@MIL-100(Fe) composites was ascribed to the MIL-100(Fe) confinement effect, with no apparent structural or morphological changes after five cycles of reuse, pointing out its stability in the long term. The catalytic performance of Pd@MIL-100(Fe) was also compared with the commercially available Pd/C catalyst and others previously tested similar catalysts, being comparable or even higher than other metal/MOFs systems reported in the literature. For this finding, the authors highlight the role of the porosity of MIL-100(Fe) in mass transfer of 4-nitrophenol molecules, leading to readily accessible PdNPs. As for the reaction mechanism, there is a hydrogen and electrons transfer from the borohydride ions to the PdNPs, that will attack 4-nitrophenol, reducing it to 4-aminophenol (Figure 30, right). The enhanced catalytic activity of Pd@MIL-100(Fe) nanocomposites was therefore ascribed to a synergistic effect between MIL-100(Fe) and PdNPs.

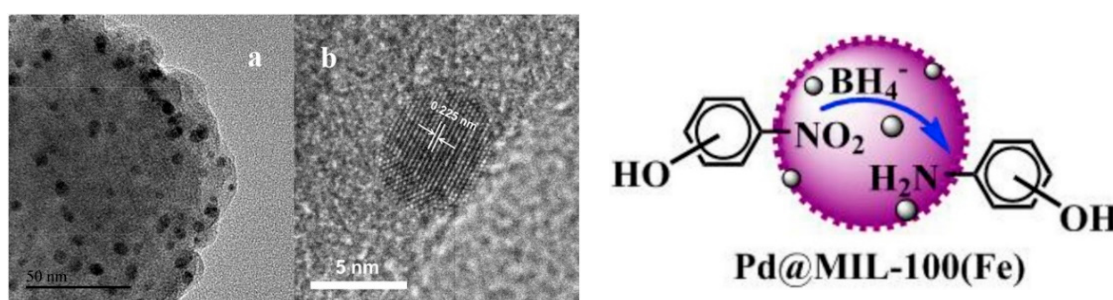


**Figure 30.** Left: (a) HRTEM image of Pd@MIL-100(Fe), (b) lattice fringe of the (111) plane of face-centered cubic Pd. Right: proposed mechanisms of nitrophenol reduction by Pd@MIL-100(Fe). Reproduced with permission from Xu et al., *Microporous and Mesoporous Materials*; published by Elsevier Inc., 2017.

In 2014, an easy synthesis procedure for the encapsulation of PdNPs through ligand design preceding the UiO-67 MOF assembly was reported for the first time by Chen et al. [97]. The choice of a UiO-67 type MOF was due to its textural parameters and extraordinary stability [98]. A mixed ligand strategy was used for the synthesis of Pd-UiO-67, using  $\text{PdCl}_2(\text{CH}_3\text{CN})_2$  and dimethyl (2,20-bipyridine)-5,50-dicarboxylate as ligand, followed by base-catalyzed hydrolysis. The prepared Pd(II)-in-UiO-67 was reduced yielding Pd(0)-in-UiO-67, with different Pd loadings (Figure 31). Pd was also immobilized on the pre-synthesized UiO-67 by means of an impregnation method obtaining Pd0/UiO-67, for comparison purposes.

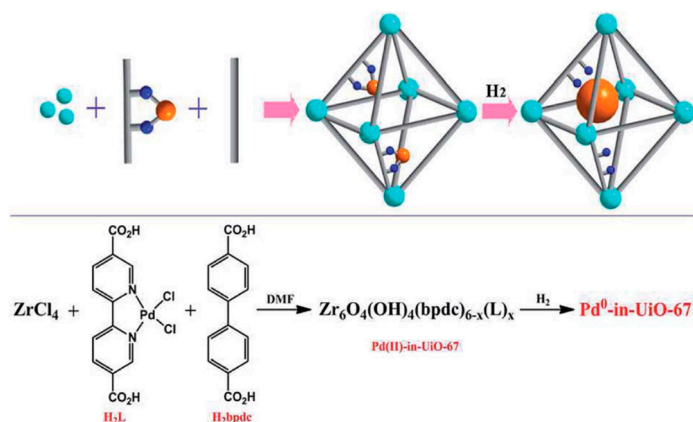


**Figure 31.** Scheme of the synthesis of Pd0-in-UiO-67. Color code: cyan, secondary building unit of MOFs; grey, organic linkers; orange, metal precursors or NPs; red, stabilizing agents. Reproduced with permission from Chen et al. [99], *Chemical Science*; published by Royal Society of Chemistry, 2014.



No crystallinity loss was observed for the Pd modified samples, suggesting the integrity of the UiO-67 structure after modification. Nitrogen adsorption isotherms pointed out the occupation of the cavities of UiO-67 by the highly dispersed PdNPs. The slight surface area decrease for Pd(0)-in-UiO-67 was probably due to Pd introduction by ligand design preceding MOF assembling. The aggregation of metal precursors was therefore significantly restricted, contrarily to reports in the literature for the posterior introduction of Pd [100]. A PdNPs uniform distribution throughout the UiO-67 framework was observed for 1.0% Pd0-in-UiO-67, for 3.0 nm particles, mostly located inside UiO-67 (Figure 32). Additionally, the presence of Pd(0) in Pd0-in-UiO-67 was confirmed. TEM images of Pd0/UiO-67 revealed 5.5 nm PdNPs, with some aggregation and deposition on the external surface. Moreover, FTIR spectra showed electron transfer from UiO-67 to PdNPs, proving a clear interaction between the two.

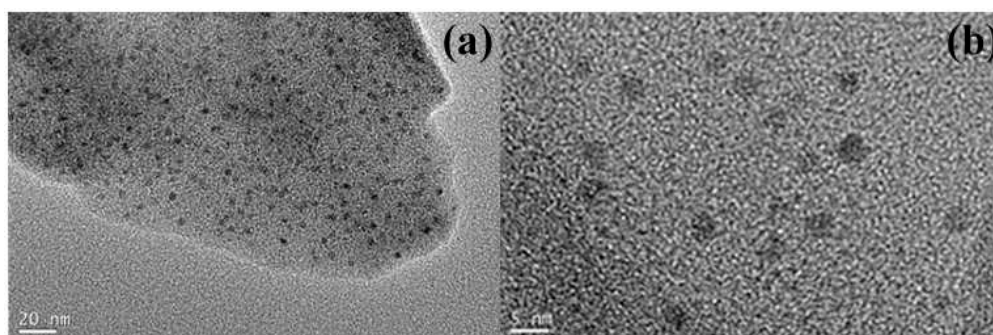


**Figure 32.** (a) and (b) TEM images of 1.0% Pd0-in-UiO-67. Reproduced with permission from Chen et al., *Chemical Science*; published by Royal Society of Chemistry, 2014.

Pd(0)-in-UiO-67 and 0.6% Pd0/UiO-67 were applied in the hydrogenation of styrene and tetraphenylethylene. Both the catalysts demonstrated high activity towards styrene hydrogenation, presenting similar conversion, indicating no significant diffusional issues for UiO-67 framework, due to the styrene small dimensions (4.2 Å). On the contrary, for the hydrogenation of a bulkier molecule (tetraphenylethylene, 6.7 Å), significantly different results were obtained, with no detectable activity for Pd0-in-UiO-67, and a comparably good activity for Pd0/UiO-67 catalyst.

These results demonstrated that PdNPs located on the external surface play a key role in the reaction in comparison to the encapsulated PdNPs due to pore size exclusion. The encapsulated PdNPs showed very good shape-selectivity, showing significantly enhanced catalytic activities and stability for the hydrogenation of olefins and nitrobenzene reduction. In brief, the enhanced catalytic activity and stability were attributed to the confinement effect and electron-donation provided by the geometry of the MOF [97].

The influence of the chemical environment of PdNPs on their catalytic performance was investigated by Chen et al. Therein, Pd@UiO-66-X composites were prepared by PdNPs encapsulation via an ultrasound-assisted double-solvent approach into the pores of MOF UiO-66-X (X = H, OMe, NH<sub>2</sub>, 2OH, 2OH(Hf)) (Figure 33) [99]. UiO-66-X presents a 3D network consisting in two types of small diameters cages and high chemical stability [98,101]. XRD patterns of UiO-66-X and Pd@UiO-66-X confirmed its crystallinity and all Pd@UiO-66-X appear to have inherited the UiO-66 structure. A surface area decrease upon the introduction of different functional groups on Pd@UiO-66-X was observed, due to the partial pore occupation and increased PdNPs weight. All Pd@UiO-66-X catalysts display analogous pore size distributions, thus allowing the exclusive study of the influence of the chemical environment. TEM images for Pd@UiO-66-NH<sub>2</sub> suggests that very small PdNPs (<1.1 nm) are highly dispersed throughout the entire MOF particle, further confirmed by the EDS mapping. Most of PdNPs presenting similar or inferior dimensions regarding the MOF cages were effectively confined. The Pd contents in Pd@UiO-66-X lie in the range of 2.1–2.8 wt%.

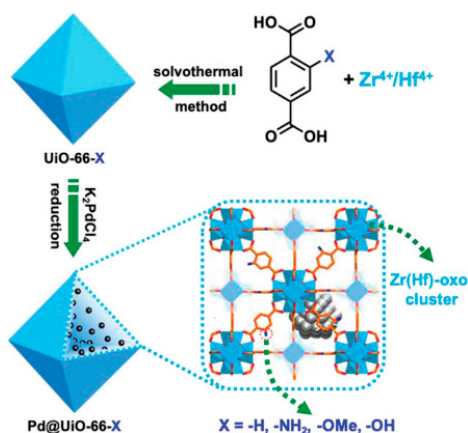


**Figure 33.** Schematic illustration of the preparation of Pd@UiO-66-X. Reproduced with permission from Chen et al., *Advanced Materials*; published by Wiley-VCH Verlag & Co. KGaA, Weinheim, Germany, 2020.

The selective hydrogenation of benzoic acid was explored for the prepared catalysts. The Pd@UiO-66-X have shown quite a distinctive catalytic activity, regarding the corresponding functional group and metal cluster (Figure 34). The almost complete conversion (>99%) for Pd@UiO-66-2OH contrasts with the increasingly decreased conversions obtained for Pd@UiO-66-NH<sub>2</sub>, Pd@UiO-66-OMe, and Pd@UiO-66, of 73, 30, and 7%, respectively. Nevertheless, all the catalysts were able to convert benzoic acid with total selectivity to benzyl alcohol and more importantly, conserved integrity of the UiO-66-2OH structure, without Pd agglomeration.

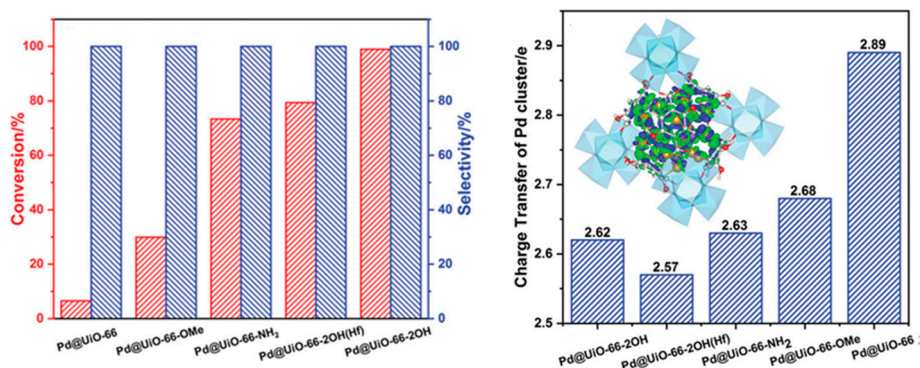


**Figure 34.** Left: Conversion and selectivity performance of Pd@UiO-66-X towards hydrogenation of benzoic acid. Right: Electron transfer from Pd clusters to the MOF. Reproduced with permission from Chen et al., *Advanced Materials*; published by Wiley-VCH Verlag & Co. KGaA, Weinheim, Germany, 2020.

The surface electronic properties of confined PdNPs, regarding the discriminated charge transfer interactions among Pd and the MOF, are accountable for the results, as the number of electrons transferred from the Pd clusters to the framework is consisting with its activity (Figure 34, right). Further studies also revealed the contribution of the adsorption energy of Pd@UiO-66-X catalysts for this matter. The adsorption strength of substrates follows the sequence Pd@UiO-66-2OH < Pd@UiO-66-2OH(Hf) < Pd@UiO-66-NH<sub>2</sub> < Pd@UiO-66-OMe < Pd@UiO-66, that is, the opposite of that observed for the catalytic activity [99]. Pd@UiO-66-2OH catalyst was further explored for the hydrogenation of benzoic acid derivatives, achieving excellent conversion and selectivity for all p-substituted benzoic acids.

Zhou et al. described an effective in situ methodology for the preparation of highly stable ZIF-8 supported carbon-stabilized PdNPs (C@Pd/ZIF-8) [102]. ZIF-8 is a typical MOF presenting a

well-defined porous structure with high surface area and large pore size and also high thermal stability, being selected as the support to disperse the carbon encapsulated PdNPs (Figure 35).

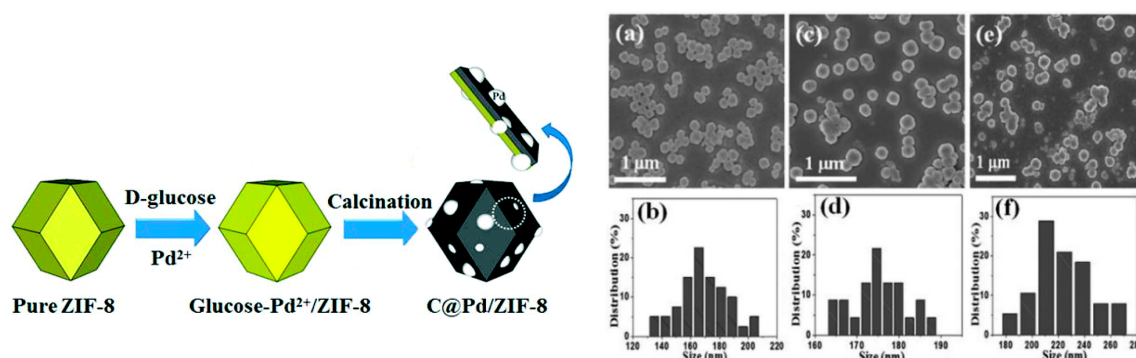


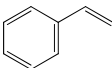
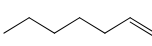
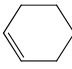
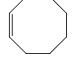
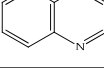
**Figure 35.** Left: Synthetic procedure for C@Pd/ZIF-8 catalysts; Right: SEM images and particle size distribution of ZIF-8 (a,b), Pd/ZIF-8 (c,d), and C@Pd/ZIF-8 (e,f) (right). Adapted with permission from Zhou et al., *Nanoscale*; published by Royal Society of Chemistry, 2015.

Glucose and Pd salts introduced into the porous structure of ZIF-8 were further converted to the resultant carbon and PdNPs. The growth of the stable carbon-encapsulated PdNPs was controlled by both the neighboring carbon and the porosity of ZIF-8, providing good dispersion without aggregation and high stability.

As estimated, C@Pd/ZIF-8 presented a decrease of the surface area compared to pure ZIF-8 owing to the residual carbon. Pore size distributions for both materials centered at ~2 nm, thus large enough for substrates access within the cavities. XRD patterns and FTIR spectra suggested a well-preserved structure for ZIF-8 in the C@Pd/ZIF-8 catalysts. In addition, SEM images disclose similar morphologies, although with different sizes (Figure 35). The larger size of the C@Pd/ZIF-8 comparing to the synthesized ZIF-8, was related to the amorphous carbon on the surface of ZIF-8, upon decomposition of glucose. Well-dispersed PdNPs were observed by TEM, presenting particle sizes of around 1.7 and 2.7 nm for Pd/ZIF-8 and C@Pd/ZIF-8, respectively. The determined Pd content in Pd/ZIF-8 and C@Pd/ZIF-8 was of about 2.9% and 2.7%, respectively.

C@Pd/ZIF-8 catalysts were used in the hydrogenation of olefins (Table 10). The high activity of the C@Pd/ZIF-8 catalysts was corroborated, and also a significantly enhanced recycling stability when compared to Pd/ZIF-8.

**Table 10.** Catalytic activity of the catalysts towards the hydrogenation of olefins [103].

Substrate	Conversion (%)	
	C@PdZIF-8	Pd/ZIF-8
	95.1	98.5
	75.2	77.8
	47.3	44.9
	24.7	21.8
	19.6	17.7

Both catalysts exhibited analogous conversions yield in the hydrogenation of olefins. Recycling studies for C@Pd/ZIF-8 and Pd/ZIF-8 towards the hydrogenation of olefins were conducted, revealing a successful reuse of C@Pd/ZIF-8 in five consecutive cycles without significant catalytic activity loss. Conversion yields of 85, 67, and 38% were obtained for the hydrogenations of styrene, 1-heptene, and cyclohexene, in the fifth run. For Pd/ZIF-8, an accentuated drop in the activity was observed after each cycle. TEM images of the recycled C@Pd/ZIF-8 catalyst showed an unchanged mean diameter for the PdNPs compared to the fresh catalyst. Quite the opposite occurred for Pd/ZIF-8, with an accentuated decrease on conversion during the recycles, most likely related to serious aggregation or leaching, resulting in catalyst deactivation. The commercially available Pd/C catalyst demonstrated poor stability in comparison with C@Pd/ZIF-8.

In 2020, Zhao and co-workers reported a simple and sustainable method using ZIF-8 for the preparation of Pd@ZIF-8 hollow microspheres with encapsulated PdNPs [103], highlighting once again the great catalytic potential of this material. The proposed procedure avoided the use of surface treatment of template microspheres. The synthesis of Pd@ZIF-8 hollow microspheres is presented in Figure 36. Well-defined Pd@ZIF-8 hollow microspheres were achieved after the removal of the polyvinylpyrrolidone (PVP)-stabilized polystyrene (PS) template microspheres. SEM and TEM images exhibited monodispersed 1.3  $\mu\text{m}$  PS template and small PdNPs (ca. 4.5 nm) well dispersed on the microspheres, with no signs of visible aggregation. SEM images demonstrated the encapsulation of every PS/Pd composite particle by a ZIF-8 shell (ca. 120 nm) (Figure 37). The Pd@ZIF-8 hollow microspheres, with a Pd content of 1.86%, presented a spherical shape and uniform size, maintaining its integrity. The textural parameters point out the microporosity of the ZIF-8 shell, with micropores with widths in the range of 1–2 nm. The slight decrease in the surface area observed for Pd@ZIF-8 hollow microspheres did not cause diffusional constraints to the reactants in the catalytic process.

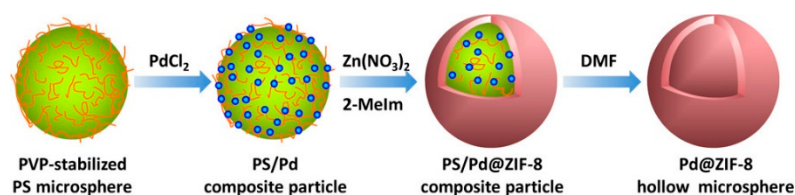


**Figure 36.** Synthetic procedure of Pd@ZIF-8 hollow microspheres. Reproduced with permission from Zhao et al., *Langmuir*; published by The American Chemical Society, 2020.

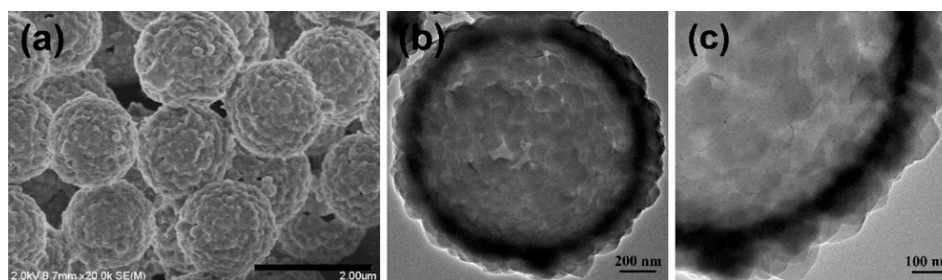


**Figure 37.** SEM image (a) and TEM images (b,c) of the Pd@ZIF-8 hollow microspheres with the diameter of PdNPs being ca. 7.0 nm. Reproduced with permission from Zhao et al., *Langmuir*; published by The American Chemical Society, 2020.

The tuning of the structure of Pd@ZIF-8 hollow microspheres was accomplished by the regulating effect of the shell thickness of ZIF-8. The PS/Pd composite particles containing smaller sized PdNPs have shown higher catalytic activity, pointing out the role of PdNPs functions as catalytically active sites in the composite.



Pd@ZIF-8 hollow microspheres, PS/Pd, and PS/Pd@ZIF-8 composite particles were assessed for the hydrogenation of alkenes of different molecular sizes in liquid-phase. Selected data of the catalytic performance of the materials is presented in Figure 38. The three catalysts demonstrated high activity for 1-hexene hydrogenation, reaching full conversion, given the small dimensions of this molecule (2.5 Å), and the absence of diffusional constraints through the pore openings of ZIF-8 shells (3.4 Å). In the case of cyclohexene (4.2 Å), while the PS/Pd composite yet demonstrated significant activity and conversion, a dramatic conversion decrease was reported for the PS/Pd@ZIF-8 (13%) and Pd@ZIF-8 (16%) as catalysts, respectively. Although cyclohexene dimensions surpassed the aperture size of ZIF-8, diffusion of this molecule was still possible, due to the framework flexibility. No visible activity was observed for the hydrogenation of cyclooctene for the PS/Pd@ZIF-8 composite particles and Pd@ZIF-8 hollow microspheres. However, the PS/Pd composite particles showed 22% of cyclooctene conversion. Cyclooctene (5.5 Å) is considerably larger than the aperture size of ZIF-8, and therefore, only PS/Pd composite particles with anchored PdNPs on the surface of PS microspheres have shown catalytic activity. These findings demonstrate the role of molecular sieve played by Pd@ZIF-8 for selective catalysis. Recycling studies for the Pd@ZIF-8 hollow microspheres towards 1-hexene hydrogenation were conducted. The catalyst maintained its activity, with a slight drop in the conversion of 1-hexene, with an unchanged morphology after three cycles, with almost no aggregation of the PdNPs (Figure 38).

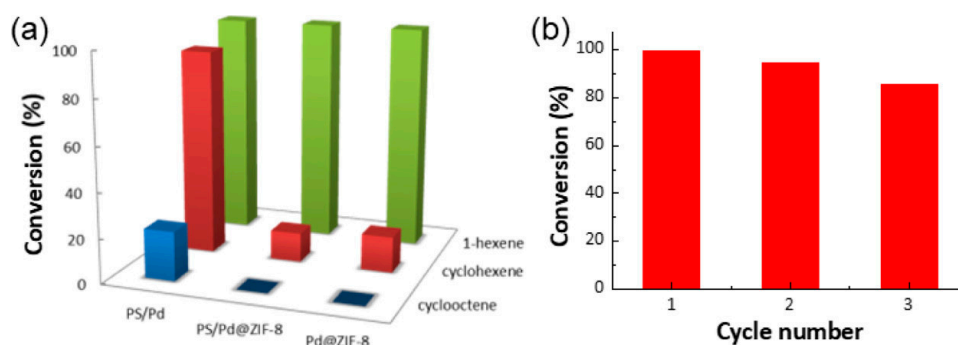


**Figure 38.** (a) Catalytic performance of PS/Pd composite particles, PS/Pd@ZIF-8 composite particles, and Pd@ZIF-8 hollow microspheres for the hydrogenation of 1-hexene, cyclohexene, and cyclooctene in the liquid phase. (b) Recycling stability of Pd@ZIF-8 hollow microspheres in the hydrogenation of 1-hexene. Reproduced with permission from Zhao et al., *Langmuir*; published by The American Chemical Society, 2020.

Summarizing, we here present an overview of the most significant findings on the catalytic performance regarding the supported catalysts discussed above towards hydrogenation reactions (Table 11). Nonetheless, it is important to emphasize that the comparison between reported results is not straightforward, as the reactions, experimental conditions, and studied parameters can be quite distinct from case to case.



**Table 11.** Selected data for the catalytic activity of PdNPs supported catalysts towards hydrogenation reactions discussed in this review.

Support	Catalyst	Substrate	Major Outcomes	Ref.
Silicas	Pd-MS-xx-TMB	chloronitrobenzenes	The role of TMB as an efficient expanding and structure-directing agent was investigated for the Pd-MS catalysts. Full conversion of <i>p</i> -CNB with a 99.9% selectivity towards <i>p</i> -chloroaniline was observed for Pd-MS-50-TMB. The enhanced activity was attributed to the larger porosity and to the morphology of the support, which enhances mass transfer. TMB catalyst displayed high stability and thermal resistance.	[38]
	Silica-based nanotubes supported PdNPs	$\alpha,\beta$ -unsaturated carboxylic acids	Mesoporous silica-based nanotubes with PdNPs uniformly dispersed were obtained. The catalysts afforded >99% conversion of benzyl alcohol and 89% selectivity to benzaldehyde, as result of the surface hydrophobic/hydrophilic properties, and nanotube morphology.	[41]
	APPd(0)@Si BPPd(0)@Si	trans-cinnamic acid and related compounds	Green synthesis of Pd(0) catalysts using modified of reverse phase silica, that facilitated metal anchorage. Effective catalysts for hydrogenation of various unsaturated olefins, with excellent recyclability. Product yields above 95% were observed for the hydrogenation of all of the unsaturated esters, ketones, and alcohols in the liquid phase.	[44]
	Pd/MCM-41-SiO <sub>2</sub> Pd/MCM-41-silatrane	polyunsaturated fatty acid methyl esters	Rapidly and selective conversion. Pd/MCM-41-silatrane has higher activity. The silica source and the Pd amount modified the active sites and size distribution of PdNPs determining the catalytic reactivity and selectivity.	[45]
	Pd/SBA-COOH	nitrobenzene	A synergistic effect is observed between the SBA-COOH support and its texture for the particle size control and distribution of PdNPs. Selectivity to nitroaniline reached 100% in all cases.	[47]
Carbons	PdNPs/RGO	nitrobenzene	Green in-situ approach using diverse reducing agents. Pd/RGO-salicylic acid exhibited distinct catalytic activity, affording 100% of nitrobenzene conversion, being reused for two times.	[58]
	PdNPs/RGO	nitroaromatics	Green synthesis through reduction of GO and Pd <sup>2+</sup> ions using barberry fruit extract. The catalysts afforded excellent product yield (>95%) for a wide selection of substrates and good catalyst recycling.	[59]
	Pd@C/CNT	acetylene	Core-shell structure Pd@C NP CNTs-supported benefited from an N-doped carbon, enhancing the stability of PdNPs, and modifying the electronic structure of PdNP. Pd@C/CNTs presented high selectivity and excellent stability.	[10]
	CPG (composite PdNPs graphene)	nitroarenes	Synthesized by a facile route, catalyst presents excellent activity (product yield >99%) and stability for the selective reduction of nitro groups with high yields, ascribed to the synergism between the ultrafine PdNPs and GO support.	[62]
	Pd@Hal-Char	nitroarenes	The use of a catalytic amount of $\beta$ -cyclodextrin significantly improved the reaction yield, reaching 100% in the best case. Hal-Char was more effective as a support than each component individually. PdNPs size and dispersion affected the catalytic activity.	[63]
	Pd@HCh	alkynes, alkenes, and carbonyl and nitro derivatives	Bio-sourced PdNPs supported on chars derivatized with ether linkers containing ammonium groups. The latter exhibited high activity in hydrogenations of several substrates, with full hydrogenation of alkyne and alkene substrates. Furthermore, aldehyde and nitro groups were too hydrogenated. The most efficient catalyst was reused ten times outperforming the commercial catalyst.	[64]

Table 11. Cont.

Support	Catalyst	Substrate	Major Outcomes	Ref.
Zeolites	Pd/ZSM-5-IS	<i>p</i> -nitrophenol	In-situ synthesis of Pd/ZSM-5-IS, with highly dispersed and small sized PdNPs, showing high catalytic activity, with almost full substrate conversion and remarkable recycle stability. Most of PdNPs were confined within ZSM-5, prevented aggregation and sintering.	[76]
	Pd@Beta	nitroarenes	The fixation of PdNPs inside Beta zeolite crystals (Pd@Beta) was the key for superior selectivity to the nitro group (for example, 99% selectivity to 4-amino-acetophenone). The outstanding selectivity of Pd@Beta was due to the sterically adsorption on the PdNPs controlled by the zeolite micropores.	[67]
	Pd@mnc-S1	nitrobenzene	A one-pot method was used for PdNPs encapsulation. Excellent stability and activity were observed for the catalyst, due to its unique porosity and nanostructure that provided general shape-selectivity for selective hydrogenation reactions. A conversion of 94% was achieved over Pd@mnc-S1.	[79]
	Pd@S-1-OH	furfural	A novel approach for selective hydrogenation using a core-shell Pd@S-1 zeolite catalyst with well-regulated wettability of the zeolite cover. Influence of the hydrophilicity of the microporosity of the zeolite on the diffusion of various molecules was discussed. Catalysts show outstanding activity, selectivity, and stability in furfural hydrogenation, showing furan selectivity as high as 99.9% with a complete conversion of furfural.	[81]
	Pd@FER	1-hexene 1-phenyl-1-cyclohexene	Remarkable shape-selectivity in the catalytic hydrogenation of different molecular sizes olefins, or steric hindrance due to nanostructure and microporosity of the catalyst. Full conversion was achieved for 1-hexene.	[83]
MOFs	Pd@Beta Pd@MWW	nitroarenes	Electronic/steric effects were accountable for the catalytic activity, with catalyst being less active for nitroarenes containing an electron-withdrawing substituent. The ortho isomers are more difficult to reduce due to steric hindrance effect. Full conversion was observed for 3-nitrotoluene and 3-nitroanisole.	[84]
	Pd@MIL-101 Pd@MIL-53	phenol	The effect of framework structure of Pd@MOFs was studied. MIL-101 was a better support, due to its mesoporosity and hydrophilicity. Larger PdNPs on the external surface of MIL-53. Both catalysts provided high selectivity (>98%) to cyclohexanone. The catalysts were recycled 5 times.	[89]
	Pd@MIL-100(Fe)	nitrophenols	Facile synthesis of Pd@MIL-100(Fe) with uniform morphology and size. The confinement effect leads to high stability within the MIL-100(Fe). High catalytic activity (conversion > 95%) and reusability due to the synergism effect amongst PdNPs and MIL-100(Fe).	[95]
	Pd(0)-in-UiO-67	styrene and tetraphenylethylene	Facile and efficient strategy for Pd@MOF catalysts via controllable introduction of Pd precursors prior to MOF assembly. Catalysts were highly active due to electron donation and confinement effects. High stability and reusability. Full conversion of styrene was reported.	[97]
	Pd@UiO-66-X	benzoic acid	Modulation of the surface microenvironment of the MOF via group functionalization and metal substitution. The activity is assigned to charge transfer processes, and to the adsorption energy of the substrate. Pd@UiO-66-2OH, which features a moderate adsorption energy and a high Pd electronic state, has shown the highest activity (>99%). Selectivity to benzyl alcohol was >99% in all cases.	[100]
	C@Pd/ZIF-8	olefins	Preparation of ZIF-8 supported C-stabilized PdNPs through an effective strategy. Due to efficient stabilization, the controlled sized PdNPs can be well dispersed onto the ZIF-8. High activity in the hydrogenation of olefins (95%) and a satisfactory reuse in 5 cycles.	[102]
	Pd@ZIF-8 hollow microspheres	alkenes	A green approach for Pd@ZIF-8 hollow microspheres preparation, uniform in size, with good structural stability, high catalytic activity and size selectivity towards the hydrogenation of alkenes (full conversion for 1-hexene), and good recycling stability.	[103]

## 8. Conclusions

In light of the findings discussed in this review, the immobilization of PdNPs in solid supports is a hot topic among the research community, especially in catalytic processes. Recent advances concerning the design and preparation of supported PdNPs have proved that a plentiful diversity of preparation methodologies and numerous supports with tailored size and distribution contribute to activity, selectivity, and recyclability of the catalytic systems, overcoming the drawbacks of traditional synthetic approaches. The development of immobilized PdNPs is unequivocally a significant theme in the field of nanomaterials. Development in this area will continue in order to combine efforts towards new facile, in-situ, sustainable, and consistent procedures to allow a practical application in industrial catalytic processes in the future. In parallel, the use of biomass-derived materials as supports for PdNPs will most definitely continue to increase, regardless of the many challenges that are posed for these approaches.

**Author Contributions:** Writing—original draft preparation, M.A.A.; writing—review and editing, M.A.A. and L.M.D.R.S.M. All authors have read and agreed to the published version of the manuscript.

**Funding:** This research was partially funded by FCT through UIDB/00100/2020 of Centro de Química Estrutural. M.A.A. acknowledges financial support from UID/QUI/00100/2019-BL/CQE-2017-022 FCT grant.

**Conflicts of Interest:** The authors declare no conflict of interest.

## References

1. Zaera, F. Nanostructured materials for applications in heterogeneous catalysis. *Chem. Soc. Rev.* **2013**, *42*, 2746–2762. [CrossRef] [PubMed]
2. Poole, C.P., Jr.; Owens, F.J. *Introduction to Nanotechnology*; John Wiley & Sons: Hoboken, NJ, USA, 2003.
3. Philippot, K.; Serp, P. Concepts in Nanocatalysis. In *Nanomaterials in Catalysis: First Edition*; Wiley-VCH Verlag GmbH & Co KGaA: Weinheim, Germany, 2013; pp. 1–54. ISBN 9783527331246.
4. Narayan, N.; Meiyazhagan, A.; Vajtai, R. Metal nanoparticles as green catalysts. *Materials* **2019**, *12*, 3602. [CrossRef] [PubMed]
5. Fedlheim, D.; Foss, C. *Metal Nanoparticles: Synthesis, Characterization, and Applications*; Marcel Dekker, Inc.: New York, NY, USA, 2002.
6. Sharma, N.; Ojha, H.; Bharadwaj, A.; Pathak, D.P.; Sharma, R.K. Preparation and catalytic applications of nanomaterials: A review. *RSC Adv.* **2015**, *5*, 53381–53403. [CrossRef]
7. White, R.J.; Luque, R.; Budarin, V.L.; Clark, J.H.; Macquarrie, D.J. Supported metal nanoparticles on porous materials. Methods and applications. *Chem. Soc. Rev.* **2009**, *38*, 481–494. [CrossRef] [PubMed]
8. Catalytic Hydrogenation, Volume 27-1st Edition. Available online: <https://www.elsevier.com/books/catalytic-hydrogenation/cerveny/978-0-444-42682-6> (accessed on 25 July 2020).
9. Johnstone, R.A.W.; Wilby, A.H.; Entwistle, I.D. Heterogeneous Catalytic Transfer Hydrogenation and Its Relation to Other Methods for Reduction of Organic Compounds. *Chem. Rev.* **1985**, *85*, 129–170. [CrossRef]
10. Zhang, L.; Ding, Y.; Wu, K.H.; Niu, Y.; Luo, J.; Yang, X.; Zhang, B.; Su, D. Pd@C core-shell nanoparticles on carbon nanotubes as highly stable and selective catalysts for hydrogenation of acetylene to ethylene. *Nanoscale* **2017**, *9*, 14317–14321. [CrossRef]
11. Liu, L.; Corma, A. Metal Catalysts for Heterogeneous Catalysis: From Single Atoms to Nanoclusters and Nanoparticles. *Chem. Rev.* **2018**, *118*, 4981–5079. [CrossRef]
12. Chen, Q.A.; Ye, Z.S.; Duan, Y.; Zhou, Y.G. Homogeneous palladium-catalyzed asymmetric hydrogenation. *Chem. Soc. Rev.* **2013**, *42*, 497–511. [CrossRef]
13. Bulut, S.; Fei, Z.; Siankevich, S.; Zhang, J.; Yan, N.; Dyson, P.J. Aqueous-phase hydrogenation of alkenes and arenes: The growing role of nanoscale catalysts. *Catal. Today* **2015**, *247*, 96–103. [CrossRef]
14. Wang, D.; Astruc, D. The Golden Age of Transfer Hydrogenation. *Chem. Rev.* **2015**, *115*, 6621–6686. [CrossRef]
15. Andrade, M.A.; Mestre, A.S.; Carvalho, A.P.; Pombeiro, A.J.L.; Martins, L.M.D.R.S. The role of nanoporous carbon materials in catalytic cyclohexane oxidation. *Catal. Today* **2019**, 1–10. [CrossRef]

16. Grau-Atienza, A.; Campos, R.; Serrano, E.; Ojeda, M.; Romero, A.A.; Garcia-Martinez, J.; Luque, R. Insights into the active species of Nanoparticle-functionalized hierarchical zeolites in alkylation reactions. *ChemCatChem* **2014**, *6*, 3530–3539. [\[CrossRef\]](#)
17. Andrade, M.A.; Martins, L.M.D.R.S. Sustainability in catalytic cyclohexane oxidation: The contribution of porous support materials. *Catalysts* **2020**, *10*, 2. [\[CrossRef\]](#)
18. Zhang, P.; Zhu, H.; Dai, S. Porous Carbon Supports: Recent Advances with Various Morphologies and Compositions. *ChemCatChem* **2015**, *7*, 2788–2805. [\[CrossRef\]](#)
19. Zhai, Y.; Zhu, Z.; Dong, S. Carbon-Based Nanostructures for Advanced Catalysis. *ChemCatChem* **2015**, *7*, 2806–2815. [\[CrossRef\]](#)
20. Brunel, D.; Blanc, A.C.; Galarneau, A.; Fajula, F. New trends in the design of supported catalysts on mesoporous silicas and their applications in fine chemicals. *Catal. Today* **2002**, *73*, 139–152. [\[CrossRef\]](#)
21. Thomas, A.M.; Mohan, A.; Rout, L.; Nagappan, S.; Park, S.S.; Ha, C.S. Pd nanoparticle incorporated mesoporous silicas with excellent catalytic activity and dual responsivity. *Colloids Surf. Physicochem. Eng. Asp.* **2020**, *585*, 124074. [\[CrossRef\]](#)
22. Wang, Y.; Biradar, A.V.; Asefa, T. Assembling nanostructures for effective catalysis: Supported palladium nanoparticle multicore coated by a hollow and nanoporous zirconia shell. *ChemSusChem* **2012**, *5*, 132–139. [\[CrossRef\]](#)
23. Yang, Q.; Xu, Q.; Jiang, H.L. Metal-organic frameworks meet metal nanoparticles: Synergistic effect for enhanced catalysis. *Chem. Soc. Rev.* **2017**, *46*, 4774–4808. [\[CrossRef\]](#)
24. Luo, S.; Zeng, Z.; Zeng, G.; Liu, Z.; Xiao, R.; Chen, M.; Tang, L.; Tang, W.; Lai, C.; Cheng, M.; et al. Metal Organic Frameworks as Robust Host of Palladium Nanoparticles in Heterogeneous Catalysis: Synthesis, Application, and Prospect. *ACS Appl. Mater. Interfaces* **2019**, *11*, 32579–32598. [\[CrossRef\]](#)
25. Zanon, A.; Verpoort, F. Metals@ZIFs: Catalytic applications and size selective catalysis. *Coord. Chem. Rev.* **2017**, *353*, 201–222. [\[CrossRef\]](#)
26. Tao, Y.; Kanoh, H.; Abrams, L.; Kaneko, K. Mesopore-modified zeolites: Preparation, characterization, and applications. *Chem. Rev.* **2006**, *106*, 896–910. [\[CrossRef\]](#) [\[PubMed\]](#)
27. Navlani-García, M.; Martis, M.; Lozano-Castelló, D.; Cazorla-Amorós, D.; Mori, K.; Yamashita, H. Investigation of Pd nanoparticles supported on zeolites for hydrogen production from formic acid dehydrogenation. *Catal. Sci. Technol.* **2015**, *5*, 364–371. [\[CrossRef\]](#)
28. Dams, M.; Drijkoningen, L.; De Vos, D.E.; Jacobs, P.A.; Pauwels, B.; Van Tendeloo, G. Pd-zeolites as heterogeneous catalysts in Heck chemistry. *J. Catal.* **2002**, *209*, 225–236. [\[CrossRef\]](#)
29. Coq, B. Metal-Support Interaction in Catalysis. In *Metal-Ligand Interactions in Chemistry, Physics and Biology*; Springer: Dordrecht, The Netherlands, 2000; pp. 49–71. [\[CrossRef\]](#)
30. Zhu, Q.L.; Xu, Q. Immobilization of Ultrafine Metal Nanoparticles to High-Surface-Area Materials and Their Catalytic Applications. *Chem* **2016**, *1*, 220–245. [\[CrossRef\]](#)
31. Pálincó, I. *Heterogeneous Catalysis: A Fundamental Pillar of Sustainable Synthesis*; Elsevier Inc.: Amsterdam, The Netherlands, 2017; ISBN 9780128095492.
32. Ravi, S.; Vadukumpully, S. Sustainable carbon nanomaterials: Recent advances and its applications in energy and environmental remediation. *J. Environ. Chem. Eng.* **2016**, *4*, 835–856. [\[CrossRef\]](#)
33. Favier, I.; Madec, D.; Teuma, E.; Gomez, M. Palladium Nanoparticles Applied in Organic Synthesis as Catalytic Precursors. *Curr. Org. Chem.* **2011**, *15*, 3127–3174. [\[CrossRef\]](#)
34. Villa, A.; Schiavoni, M.; Prati, L. Material science for the support design: A powerful challenge for catalysis. *Catal. Sci. Technol.* **2012**, *2*, 673–682. [\[CrossRef\]](#)
35. Gavia, D.J.; Shon, Y.S. Catalytic properties of unsupported palladium nanoparticle surfaces capped with small organic ligands. *ChemCatChem* **2015**, *7*, 892–900. [\[CrossRef\]](#)
36. Corma, A. From microporous to mesoporous molecular sieve materials and their use in catalysis. *Chem. Rev.* **1997**, *97*, 2373–2419. [\[CrossRef\]](#)
37. Taguchi, A.; Schüth, F. Ordered mesoporous materials in catalysis. *Microporous Mesoporous Mater.* **2005**. [\[CrossRef\]](#)
38. Yu, W.; Lin, H.W.; Tan, C.S. Direct synthesis of Pd incorporated in mesoporous silica for solvent-free selective hydrogenation of chloronitrobenzenes. *Chem. Eng. J.* **2017**, *325*, 124–133. [\[CrossRef\]](#)

39. Jiang, L.; Gu, H.; Xu, X.; Yan, X. Selective hydrogenation of o-chloronitrobenzene (o-CNB) over supported Pt and Pd catalysts obtained by laser vaporization deposition of bulk metals. *J. Mol. Catal. A Chem.* **2009**, *310*, 144–149. [\[CrossRef\]](#)
40. Liu, R.J.; Crozier, P.A.; Smith, C.M.; Hucul, D.A.; Blackson, J.; Salaita, G. Metal sintering mechanisms and regeneration of palladium/alumina hydrogenation catalysts. *Appl. Catal. A Gen.* **2005**, *282*, 111–121. [\[CrossRef\]](#)
41. Sun, J.; Wang, H.; Gao, X.; Zhu, X.; Ge, Q.; Liu, X.; Han, J. Mesoporous silica-based nanotubes loaded Pd nanoparticles: Effect of framework compositions on the performance in heterogeneous catalysis. *Microporous Mesoporous Mater.* **2017**, *247*, 1–8. [\[CrossRef\]](#)
42. Liu, X.; Li, X.; Guan, Z.; Liu, J.; Zhao, J.; Yang, Y.; Yang, Q. Organosilica nanotubes: Large-scale synthesis and encapsulation of metal nanoparticles. *Chem. Commun.* **2011**, *47*, 8073–8075. [\[CrossRef\]](#) [\[PubMed\]](#)
43. Guan, Z.; Lu, S.; Li, C. Enantioselective hydrogenation of  $\alpha,\beta$ -unsaturated carboxylic acid over cinchonidine-modified Pd nanoparticles confined in carbon nanotubes. *J. Catal.* **2014**, *311*, 1–5. [\[CrossRef\]](#)
44. Shabbir, S.; Lee, S.; Lim, M.; Lee, H.; Ko, H.; Lee, Y.; Rhee, H. Pd nanoparticles on reverse phase silica gel as recyclable catalyst for Suzuki-Miyaura cross coupling reaction and hydrogenation in water. *J. Organomet. Chem.* **2017**, *846*, 296–304. [\[CrossRef\]](#)
45. Na Rungsi, A.; Luengnaruemitchai, A.; Wongkasemjit, S.; Chollacoop, N.; Chen, S.Y.; Yoshimura, Y. Influence of silica sources on structural property and activity of Pd-supported on mesoporous MCM-41 synthesized with an aid of microwave heating for partial hydrogenation of soybean methyl esters. *Appl. Catal. A Gen.* **2018**, *563*, 80–90. [\[CrossRef\]](#)
46. Chung, S.H.; Park, Y.M.; Kim, M.S.; Lee, K.Y. The effect of textural properties on the hydrogenation of succinic acid using palladium incorporated mesoporous supports. *Catal. Today* **2012**, *185*, 205–210. [\[CrossRef\]](#)
47. Ganji, S.; Bukya, P.; Liu, Z.W.; Rao, K.S.R.; Burri, D.R. A carboxylic acid functionalized SBA-15 supported Pd nanocatalyst: An efficient catalyst for hydrogenation of nitrobenzene to aniline in water. *New J. Chem.* **2019**, *43*, 11871–11875. [\[CrossRef\]](#)
48. Karimi, B.; Abedi, S.; Clark, J.H.; Budarin, V. Highly efficient aerobic oxidation of alcohols using a recoverable catalyst: The role of mesoporous channels of SBA-15 in stabilizing palladium nanoparticles. *Angew. Chem.-Int. Ed.* **2006**, *45*, 4776–4779. [\[CrossRef\]](#) [\[PubMed\]](#)
49. Saidulu, G.; Anand, N.; Rao, K.S.R.; Burri, A.; Park, S.E.; Burri, D.R. Cu/SBA-15 is an efficient solvent-free and acid-free catalyst for the rearrangement of benzaldoxime into benzamide. *Catal. Lett.* **2011**, *141*, 1865–1871. [\[CrossRef\]](#)
50. Thommes, M.; Kaneko, K.; Neimark, A.V.; Olivier, J.P.; Rodriguez-Reinoso, F.; Rouquerol, J.; Sing, K.S.W. Physisorption of gases, with special reference to the evaluation of surface area and pore size distribution (IUPAC Technical Report). *Pure Appl. Chem.* **2015**, *87*, 1051–1069. [\[CrossRef\]](#)
51. Saikia, D.; Huang, Y.Y.; Wu, C.E.; Kao, H.M. Size dependence of silver nanoparticles in carboxylic acid functionalized mesoporous silica SBA-15 for catalytic reduction of 4-nitrophenol. *RSC Adv.* **2016**, *6*, 35167–35176. [\[CrossRef\]](#)
52. Pérez-Mayoral, E.; Calvino-Casilda, V.; Soriano, E. Metal-supported carbon-based materials: Opportunities and challenges in the synthesis of valuable products. *Catal. Sci. Technol.* **2016**, *6*, 1265–1291. [\[CrossRef\]](#)
53. Calvino-Casilda, V.; Lopez-Peinado, A.J.; Duran-Valle, C.J.; Martin-Aranda, R.M. Last decade of research on activated carbons as catalytic support in chemical processes. *Catal. Rev.* **2010**, *52*, 325–380. [\[CrossRef\]](#)
54. Mestre, A.S.; Carvalho, A.P. Nanoporous Carbon Synthesis: An Old Story with Exciting New Chapters. In *Porosity-Process, Technologies and Applications*; IntechOpen: London, UK, 2018. [\[CrossRef\]](#)
55. Machado, B.F.; Serp, P. Graphene-based materials for catalysis. *Catal. Sci. Technol.* **2012**, *2*, 54–75. [\[CrossRef\]](#)
56. Figueiredo, J.L.; Pereira, M.F. Carbon as catalyst. In *Carbon Materials for Catalysis*; Serp, P., Figueiredo, J.L., Eds.; John Wiley & Sons, Inc.: Hoboken, NJ, USA, 2009; pp. 177–217. ISBN 9780470178850.
57. Bandoz, T.J.; Ania, C.O. Surface chemistry of carbon materials. In *Activated Carbon Surfaces in Environmental Remediation*; Bandoz, T.J., Ed.; Elsevier: New York, NY, USA, 2006; pp. 159–229.
58. El-Hout, S.I.; El-Sheikh, S.M.; Hassan, H.M.A.; Harraz, F.A.; Ibrahim, I.A.; El-Sharkawy, E.A. A green chemical route for synthesis of graphene supported palladium nanoparticles: A highly active and recyclable catalyst for reduction of nitrobenzene. *Appl. Catal. A Gen.* **2015**, *503*, 176–185. [\[CrossRef\]](#)
59. Nasrollahzadeh, M.; Mohammad Sajadi, S.; Rostami-Vartooni, A.; Alizadeh, M.; Bagherzadeh, M. Green synthesis of the Pd nanoparticles supported on reduced graphene oxide using barberry fruit extract



- and its application as a recyclable and heterogeneous catalyst for the reduction of nitroarenes. *J. Colloid Interface Sci.* **2016**, *466*, 360–368. [\[CrossRef\]](#)
60. Nasrollahzadeh, M.; Maham, M.; Rostami-Vartooni, A.; Bagherzadeh, M.; Sajadi, S.M. Barberry fruit extract assisted in situ green synthesis of Cu nanoparticles supported on a reduced graphene oxide-Fe<sub>3</sub>O<sub>4</sub> nanocomposite as a magnetically separable and reusable catalyst for the O-arylation of phenols with aryl halides under ligand-free cond. *RSC Adv.* **2015**, *5*, 64769–64780. [\[CrossRef\]](#)
  61. Kovtyukhova, N.I. Layer-by-layer assembly of ultrathin composite films from micron-sized graphite oxide sheets and polycations. *Chem. Mater.* **1999**, *11*, 771–778. [\[CrossRef\]](#)
  62. Bilgicli, H.G.; Burhan, H.; Diler, F.; Cellat, K.; Kuyuldar, E.; Zengin, M.; Sen, F. Composites of palladium nanoparticles and graphene oxide as a highly active and reusable catalyst for the hydrogenation of nitroarenes. *Microporous Mesoporous Mater.* **2020**, *296*, 110014. [\[CrossRef\]](#)
  63. Sadjadi, S.; Akbari, M.; Léger, B.; Monflier, E.; Heravi, M.M. Eggplant-Derived Biochar-Halloysite Nanocomposite as Supports of Pd Nanoparticles for the Catalytic Hydrogenation of Nitroarenes in the Presence of Cyclodextrin. *ACS Sustain. Chem. Eng.* **2019**, *7*, 6720–6731. [\[CrossRef\]](#)
  64. Duarte, T.A.G.; Favier, I.; Pradel, C.; Martins, L.M.D.R.S.; Carvalho, A.P.; Pla, D.; Gómez, M. Tetraalkylammonium Functionalized Hydrochars as Efficient Supports for Palladium Nanocatalysts. *ChemCatChem* **2020**, *12*, 2295–2303. [\[CrossRef\]](#)
  65. Duarte, T.A.G.; Carvalho, A.P.; Martins, L.M.D.R.S. Styrene oxidation catalyzed by copper(II) C-scorpionates in homogenous medium and immobilized on sucrose derived hydrochars. *Catal. Today* **2019**. [\[CrossRef\]](#)
  66. Mandal, S.; Roy, D.; Chaudhari, R.V.; Sastry, M. Pt and Pd nanoparticles immobilized on amine-functionalized zeolite: Excellent catalysts for hydrogenation and heck reactions. *Chem. Mater.* **2004**, *16*, 3714–3724. [\[CrossRef\]](#)
  67. Zhang, J.; Wang, L.; Shao, Y.; Wang, Y.; Gates, B.C.; Xiao, F.S. A Pd@Zeolite Catalyst for Nitroarene Hydrogenation with High Product Selectivity by Sterically Controlled Adsorption in the Zeolite Micropores. *Angew. Chem.-Int. Ed.* **2017**, *56*, 9747–9751. [\[CrossRef\]](#)
  68. Maurya, M.R.; Kumar, A.; Costa Pessoa, J. Vanadium complexes immobilized on solid supports and their use as catalysts for oxidation and functionalization of alkanes and alkenes. *Coord. Chem. Rev.* **2011**, *255*, 2315–2344. [\[CrossRef\]](#)
  69. Corma, A. State of the art and future challenges of zeolites as catalysts. *J. Catal.* **2003**, *216*, 298–312. [\[CrossRef\]](#)
  70. Ojeda, M.; Grau-Atienza, A.; Campos, R.; Romero, A.A.; Serrano, E.; Maria Marinas, J.; García Martínez, J.; Luque, R. Hierarchical zeolites and their catalytic performance in selective oxidative processes. *ChemSusChem* **2015**, *8*, 1328–1333. [\[CrossRef\]](#) [\[PubMed\]](#)
  71. Carvalho, A.P.; Nunes, N.; Martins, A. Hierarchical Zeolites: Preparation, Properties and Catalytic Applications. In *Comprehensive Guide for Mesoporous Materials, Vol. 3: Properties and Development*; Aliofkhaezrai, M., Ed.; Nova Science Publishers, Inc.: New York, NY, USA, 2015; pp. 147–211. ISBN 978-1-63463-318-5.
  72. Feliczak-Guzik, A. Hierarchical zeolites: Synthesis and catalytic properties. *Microporous Mesoporous Mater.* **2018**, *259*, 33–45. [\[CrossRef\]](#)
  73. Paixão, V.; Monteiro, R.; Andrade, M.; Fernandes, A.; Rocha, J.; Carvalho, A.P.; Martins, A. Desilication of MOR zeolite: Conventional versus microwave assisted heating. *Appl. Catal. A Gen.* **2011**, *402*, 59–68. [\[CrossRef\]](#)
  74. Paixão, V.; Carvalho, A.P.; Rocha, J.; Fernandes, A.; Martins, A. Modification of MOR by desilication treatments: Structural, textural and acidic characterization. *Microporous Mesoporous Mater.* **2010**, *131*. [\[CrossRef\]](#)
  75. Zhu, K.; Egeblad, K.; Christensen, C.H. *Tailoring the Porosity of Hierarchical Zeolites by Carbon-Templating*; Elsevier: Amsterdam, The Netherlands, 2008; Volume 174, ISBN 9780444532961.
  76. Wang, F.; Ren, J.; Cai, Y.; Sun, L.; Chen, C.; Liang, S.; Jiang, X. Palladium nanoparticles confined within ZSM-5 zeolite with enhanced stability for hydrogenation of p-nitrophenol to p-aminophenol. *Chem. Eng. J.* **2016**, *283*, 922–928. [\[CrossRef\]](#)
  77. Ma, Z.; Zhang, L.; Chen, R.; Xing, W.; Xu, N. Preparation of Pd-B/TiO<sub>2</sub> amorphous alloy catalysts and their performance on liquid-phase hydrogenation of p-nitrophenol. *Chem. Eng. J.* **2008**, *138*, 517–522. [\[CrossRef\]](#)
  78. Dong, J.; Ma, Z.; Chen, R.; Xing, W. Preparation of Pd/Al<sub>2</sub>O<sub>3</sub> catalysts and its application in synthesis of p-aminophenol. *Ind. Catal.* **2007**, *6*, 14.

79. Cui, T.L.; Ke, W.Y.; Zhang, W.B.; Wang, H.H.; Li, X.H.; Chen, J.S. Encapsulating Palladium Nanoparticles Inside Mesoporous MFI Zeolite Nanocrystals for Shape-Selective Catalysis. *Angew. Chem. -Int. Ed.* **2016**, *55*, 9178–9182. [[CrossRef](#)]
80. Cui, T.L.; Li, X.H.; Lv, L.B.; Wang, K.X.; Su, J.; Chen, J.S. Nanoscale Kirkendall growth of silicalite-1 zeolite mesocrystals with controlled mesoporosity and size. *Chem. Commun.* **2015**, *51*, 12563–12566. [[CrossRef](#)] [[PubMed](#)]
81. Wang, C.; Liu, Z.; Wang, L.; Dong, X.; Zhang, J.; Wang, G.; Han, S.; Meng, X.; Zheng, A.; Xiao, F.S. Importance of Zeolite Wettability for Selective Hydrogenation of Furfural over Pd@Zeolite Catalysts. *ACS Catal.* **2018**, *8*, 474–481. [[CrossRef](#)]
82. Zhang, H.; Gu, X.K.; Canlas, C.; Kropf, A.J.; Aich, P.; Greeley, J.P.; Elam, J.W.; Meyers, R.J.; Dumesic, J.A.; Stair, P.C.; et al. Atomic Layer Deposition Overcoating: Tuning Catalyst Selectivity for Biomass Conversion. *Angew. Chem. -Int. Ed.* **2014**, *53*, 12132–12136. [[CrossRef](#)] [[PubMed](#)]
83. Zhao, Z.; Li, Y.; Feyen, M.; McGuire, R.; Müller, U.; Zhang, W. Pd Nanoparticles Encapsulated in FER Zeolite through a Layer Reassembling Strategy as Shape-selective Hydrogenation Catalyst. *ChemCatChem* **2018**, *10*, 2254–2259. [[CrossRef](#)]
84. Zhang, Y.; Fulajtárová, K.; Kubů, M.; Mazur, M.; Hronec, M.; Čejka, J. Electronic/steric effects in hydrogenation of nitroarenes over the heterogeneous Pd@BEA and Pd@MWW catalysts. *Catal. Today* **2020**, *345*, 39–47. [[CrossRef](#)]
85. Van Den Broek, A.C.M.; Van Grondelle, J.; Van Santen, R.A. Preparation of highly dispersed platinum particles in HZSM-5 zeolite: A study of the pretreatment process of [Pt(NH<sub>3</sub>)<sub>4</sub>]<sup>2+</sup>. *J. Catal.* **1997**, *167*, 417–424. [[CrossRef](#)]
86. Igarashi, H.; Uchida, H.; Suzuki, M.; Sasaki, Y.; Watanabe, M. Removal of carbon monoxide from hydrogen-rich fuels by selective oxidation over platinum catalyst supported on zeolite. *Appl. Catal. A Gen.* **1997**, *159*, 159–169. [[CrossRef](#)]
87. Pérez-Mayoral, E.; Matos, I.; Bernardo, M.; Fonseca, I.M. New and advanced porous carbon materials in fine chemical synthesis. Emerging precursors of porous carbons. *Catalysts* **2019**, *9*, 133. [[CrossRef](#)]
88. Juan-Alcañiz, J.; Gascon, J.; Kapteijn, F. Metal-organic frameworks as scaffolds for the encapsulation of active species: State of the art and future perspectives. *J. Mater. Chem.* **2012**, *22*, 10102–10119. [[CrossRef](#)]
89. Zhang, D.; Guan, Y.; Hensen, E.J.M.; Chen, L.; Wang, Y. Porous MOFs supported palladium catalysts for phenol hydrogenation: A comparative study on MIL-101 and MIL-53. *Catal. Commun.* **2013**, *41*, 47–51. [[CrossRef](#)]
90. Millange, F.; Serre, C.; Férey, G. Synthesis, structure determination and properties of MIL-53as and MIL-53ht: The first Cr<sup>III</sup> hybrid inorganic–organic microporous solids: Cr<sup>III</sup>(OH)·{O<sub>2</sub>C–C<sub>6</sub>H<sub>4</sub>–CO<sub>2</sub>}·{HO<sub>2</sub>C–C<sub>6</sub>H<sub>4</sub>–CO<sub>2</sub>H}<sub>x</sub>·t. *Chem. Commun.* **2002**, 822–823. [[CrossRef](#)]
91. Férey, G.; Mellot-Draznieks, C.; Serre, C.; Millange, F.; Dutour, J.; Surble, S.; Margiolaki, I. A Chromium Terephthalate-Based Solid with Unusually Large Pore Volumes and Surface Area. *Science* **2005**, *309*, 2040–2042. [[CrossRef](#)]
92. Jenkins, S.J. Aromatic adsorption on metals via first-principles density functional theory. *Proc. R. Soc. A Math. Phys. Eng. Sci.* **2009**, *465*, 2949–2976. [[CrossRef](#)]
93. Chen, A.; Zhao, G.; Chen, J.; Chen, L.; Yu, Y. Selective hydrogenation of phenol and derivatives over an ionic liquid-like copolymer stabilized palladium catalyst in aqueous media. *RSC Adv.* **2013**, *3*, 4171–4175. [[CrossRef](#)]
94. Hermannsdörfer, J.; Kempe, R. Selective palladium-loaded MIL-101 catalysts. *Chem.-A Eur. J.* **2011**, *17*, 8071–8077. [[CrossRef](#)] [[PubMed](#)]
95. Xu, B.; Li, X.; Chen, Z.; Zhang, T.; Li, C. Pd@MIL-100(Fe) composite nanoparticles as efficient catalyst for reduction of 2/3/4-nitrophenol: Synergistic effect between Pd and MIL-100(Fe). *Microporous Mesoporous Mater.* **2018**, *255*, 1–6. [[CrossRef](#)]
96. Xu, B.; Chen, Z.; Han, B.; Li, C. Glycol assisted synthesis of MIL-100(Fe) nanospheres for photocatalytic oxidation of benzene to phenol. *Catal. Commun.* **2017**, *98*, 112–115. [[CrossRef](#)]
97. Chen, L.; Chen, H.; Luque, R.; Li, Y. Metal–organic framework encapsulated Pd nanoparticles: Towards advanced heterogeneous catalysts. *Chem. Sci.* **2014**, *5*, 3708–3714. [[CrossRef](#)]

98. Cavka, J.H.; Jakobsen, S.; Olsbye, U.; Guillou, N.; Lamberti, C.; Bordiga, S.; Lillerud, K.P. A new zirconium inorganic building brick forming metal organic frameworks with exceptional stability. *J. Am. Chem. Soc.* **2008**, *130*, 13850–13851. [[CrossRef](#)]
99. Dhakshinamoorthy, A.; Garcia, H. Catalysis by metal nanoparticles embedded on metal–organic frameworks. *Chem. Soc. Rev.* **2012**, *41*, 5262–5284. [[CrossRef](#)]
100. Chen, D.; Yang, W.; Jiao, L.; Li, L.; Yu, S.H.; Jiang, H.L. Boosting Catalysis of Pd Nanoparticles in MOFs by Pore Wall Engineering: The Roles of Electron Transfer and Adsorption Energy. *Adv. Mater.* **2020**, *2000041*, 1–6. [[CrossRef](#)]
101. Biswas, S.; Van Der Voort, P. A general strategy for the synthesis of functionalised UiO-66 frameworks: Characterisation, stability and CO<sub>2</sub> adsorption properties. *Eur. J. Inorg. Chem.* **2013**, 2154–2160. [[CrossRef](#)]
102. Zhou, W.; Zou, B.; Zhang, W.; Tian, D.; Huang, W.; Huo, F. Synthesis of stable heterogeneous catalysts by supporting carbon-stabilized palladium nanoparticles on MOFs. *Nanoscale* **2015**, *7*, 8720–8724. [[CrossRef](#)] [[PubMed](#)]
103. Zhao, Y.; Ni, X.; Ye, S.; Gu, Z.G.; Li, Y.; Ngai, T. A Smart Route for Encapsulating Pd Nanoparticles into a ZIF-8 Hollow Microsphere and Their Superior Catalytic Properties. *Langmuir* **2020**, *36*, 2037–2043. [[CrossRef](#)] [[PubMed](#)]



© 2020 by the authors. Licensee MDPI, Basel, Switzerland. This article is an open access article distributed under the terms and conditions of the Creative Commons Attribution (CC BY) license (<http://creativecommons.org/licenses/by/4.0/>).